



Review

Metal-organic frameworks for photocatalytic CO₂ reduction under visible radiation: A review of strategies and applications

Ismail Issa Alkhatib^{a,1}, Corrado Garlisi^{a,1}, Mario Pagliaro^b, Khalid Al-Ali^a, Giovanni Palmisano^{a,*}

^a Department of Chemical Engineering, Khalifa University of Science and Technology - Masdar City, PO BOX 54224, Abu Dhabi, United Arab Emirates

^b Istituto per lo Studio dei Materiali Nanostrutturati, CNR, via U. La Malfa 153, 90146 Palermo, Italy

ARTICLE INFO

Keywords:

Metal-organic frameworks
Photocatalytic CO₂ reduction
Visible light
Co-catalysts
Sacrificial precursors

ABSTRACT

Metal-organic frameworks (MOFs) have emerged over the last decades as an interesting class of materials for a plethora of applications due to their flexible tunability in composition, structure and functional properties. In particular, the urgent need to convert CO₂ into useful chemical substances have led to growing attention towards these catalysts as promising candidates for CO₂ capture and storage with the ultimate aim of promoting sustainable pathways to address energy and environmental problems. This review provides an overview of the fundamental factors and recent studies of MOFs for CO₂ photoreduction, pointing out the main strategies adopted in the design and testing of innovative MOFs-based catalysts, where MOFs serve either directly as the only photoactive materials for CO₂ transformation into chemical fuels or as units of hybrid catalytic arrangements to enhance CO₂ conversion. The functionalization of MOFs is a promising approach to improve their photocatalytic activity. Their absorption of visible light can be enhanced either by modification of MOFs structure or by adjusting the organic ligands to contain reactive functional groups, through the inclusion of metal nodes with higher reduction potential, or even through a combination of both strategies. MOFs can also be used as co-catalysts along with other photocatalytic entities, resulting in MOF-based composites with enhanced CO₂ photoreduction. The performance of MOFs-based photocatalysts is analyzed in this review, with a view to emphasizing not only the advantages but also the limitations, over the more traditional semiconductors photocatalysts. At the current stage, the main challenges of these MOFs-based photocatalysts relate to the economic feasibility of industrial-scale processes and to the poor stability of these materials, which is often lost after some runs. It is hoped that this review will help the design of increasingly efficient MOF-based materials for CO₂ reduction and create the needed awareness that more work is still needed in order to be able to actualize and explore the potentials of MOFs in addressing the key issues of environmental sustainability.

1. Introduction

Over the past decades, the dependency on fossil fuels as primary energy resources led to serious environmental and energetic crises. Currently, more than 80% of the global energy consumption is dependent on fossil fuels, being driven by an increase in global population and industrialization [1,2]. This excessive exploitation led in turn to the depletion of natural fossil fuel reserves. Forecasts have demonstrated that, by the year 2040, the global energy consumption will increase by 56%, by which available fossil fuel resources will not be sufficient to cover this significant increase in energy demand [1]. Apart from decreasing the natural energy reserves, the excessive utilization of fossil fuels led to a substantial rise in CO₂ emissions, which have a pivotal role in global warming phenomenon [3–5]. The CO₂ concentration

levels in the atmosphere have exceeded 400 ppm (a 40% increase from the year 1750) rising at around 2 ppm per year [6,7].

Carbon capture and storage (CCS) has been proposed as a potential method to reduce the level of generated CO₂ emissions [8,9]. However, the associated high costs of CO₂ capture, transportation, and injection in suitable underground reservoirs, along with high energy requirements, make the feasibility of such process still limited [8]. The creation of a carbon neutral energy scheme presents a promising solution that can overcome the facets of the problem associated with fossil fuel dependency. In this scheme, the abundant CO₂ can provide a suitable raw material for a closed energy loop, where generated CO₂ emissions can be transformed into chemical fuels to balance CO₂ levels in the atmosphere [10,11].

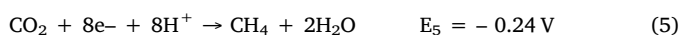
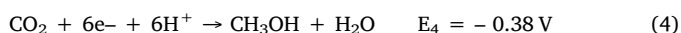
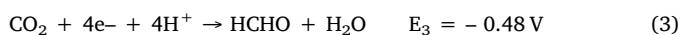
However, the prime limitation to CO₂ utilization is the high

* Corresponding author.

E-mail address: giovanni.palmisano@ku.ac.ae (G. Palmisano).

¹ Both authors contributed equally.

chemical stability of C=O bond with a dissociation energy higher than 805 kJ mol^{-1} , thus requiring a significant energy input for bond cleavage and CO_2 conversion [12,13]. Solar energy, a renewable energy resource, can be utilized for the photochemical reduction of CO_2 , by which solar energy is transformed into chemical energy in the form of chemical bonds [14,15]. The resultant products can be in the form of organic fuels such as formic acid, methanol, methane or light hydrocarbons; or fuel precursors such as CO, a syngas component [16,17]. Below are some of the most common proton-multi-electron reduction steps of CO_2 reduction in aqueous media with the corresponding electrochemical redox potentials (vs. Normal Hydrogen Electrode, pH 7) [18]:



Similar processes occur naturally in plant cells and some organisms, through photosynthesis that involves both the oxidation of water and the reduction of CO_2 . This mechanism takes place in three steps, which are light harvesting, generation of charge carriers and reduction/oxidation reactions. The plant cell naturally assembles this complex system by connecting a light-harvesting antenna network, a molecular water oxidation center and a CO_2 reduction mechanism to transform solar energy into chemical energy stored in carbohydrates or hydrogen [19]. Artificial photosynthesis can combine these mechanisms in a two- or one-step process, taking advantage of semiconductors able to trigger photocatalytic conversion. One of the earliest works on the conversion of solar energy using photocatalysts was done by Fujishima et al. in 1972 [20]. This work has demonstrated a UV-light driven water splitting for hydrogen production using TiO_2 . This discovery was followed by many efforts exploring a range of different inorganic semiconductors [21–24].

The process of photocatalytic CO_2 reduction over a semiconductor is initiated by the creation of photogenerated charge carriers (electron-hole pairs) as shown in Fig. 1. The semiconductor absorbs light upon irradiation if the energy of the absorbed light is larger than the band gap of the material; electrons in the valence band (VB) absorb enough energy to be promoted to the conduction band (CB), leaving holes in the

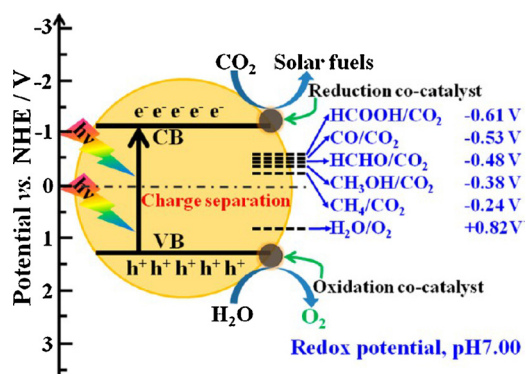


Fig. 1. Elementary steps occurring in a photocatalytic reduction of CO_2 over a semiconductor mediated by appropriate redox co-catalysts: i) light absorption, ii) electron excitation from the VB to the CB, iii) charge migration to the surface of the particle, oxidation of H_2O by the positive holes (h^+), reduction of CO_2 by multiple electrons (e^-) [18].

VB. Subsequently, the developed charge carriers are separated and mobile enough to migrate away from the site of charge separation, reaching the active sites on the surface of the catalyst to undergo subsequent reactions [25,26]. Finally, the mobile charge carriers are involved in the reduction and oxidation semi-reactions at the catalytic sites, where electrons in the conduction band partake in the CO_2 reduction reaction, while the holes in the valence band are involved in water oxidation [27].

The mobility of generated charge carriers is a crucial step in this process; the electrons might migrate to the surface active sites and undergo a surface redox reaction which is a favorable pathway. However, the electrons might also be captured by defective sites in the bulk of the semiconductors or recombine with the photogenerated holes by releasing the excess energy to the surrounding environment; both are unfavorable pathways [28,29]. The position of the band-edges dictates whether or not a semiconductor can catalyze a specific reaction. More precisely, the CB must be more negative than the reduction semireaction potential; similarly, the VB must be more positive than oxidation semireaction potential [28]. The high number of electrons (2–8) required for CO_2 reduction along with a high recombination rate of electron-hole pairs are the most dominant issues in photocatalytic CO_2 reduction [15,30]. Other challenges to overcome are low conversion rates, visible light responsiveness to exploit readily available solar energy, uncontrollable selectivity, incapability to completely suppress the competing hydrogen evolution reaction (HER) in the presence of water and low catalyst stability when exposed to other gases commonly present in flue gas (i.e., O_2) [31–33].

Hence, it is imperative to develop new photocatalytic materials with tunable functionalities to overcome the limitation of current ones. Such a material can be in the form of metal-organic frameworks (MOFs) [34], also known as coordination polymers, which are a class of crystalline micro-/meso-porous hybrid materials [35]. These crystals are composed of inorganic metal ions or clusters connected to organic moieties or ligands. The metal centers act as connecting nodes of the crystalline lattice and are fixed in place by the organic moieties working as ligands [29], through electrostatic attraction and coordinative metal-ligand interactions of moderate strength [25].

The use of MOFs for heterogeneous photocatalytic applications to operate artificial photosynthetic reactions such as water splitting, CO_2 reduction, and organic photosynthesis is very promising [36]. This is mainly due to their structural arrangement, which in principle can provide a platform that assists in the integration of the different molecular components, such as photosensitizers and catalytic centers, into a single solid material [37]. The application of MOFs as photocatalysts is based on a number of considerations. Firstly, some MOFs can behave as semiconductors mainly due to the presence of the organic ligand, as they can serve as charge carrier transporting system through the photoexcitation of organic ligands or metal clusters [38]. Upon light irradiation, the organic ligand acts as an antenna to capture photons, with electrons getting excited from the VB to the CB and being transferred to the metal nodes through a ligand-to-metal cluster charge transition mechanism (LCCT), greatly facilitated by the MOF's crystalline structure. The activated metal nodes are then involved in heterogeneous photoredox reactions [39].

Secondly, MOFs can exhibit catalytic activity due to their unsaturated metal atoms or catalytically active organic ligands [40,41]. Furthermore, the introduction of extra active sites can be done through the functionalization of the parent structures of MOFs [23]. The porous structure of MOFs can host photoactive metal complexes or dyes that have a high activity, making MOFs an ideal platform to incorporate homogenous catalytic centers and endowing them with heterogeneous catalyst-like functionality including easy separation and recycling without sacrificing their superior activity [42]. Finally, the most advantageous feature of MOFs is the ease of adjusting their chemical and physical properties through modifying their organic ligands, metal centers, active functional groups, or yet by tuning their morphology

[43,44]. Almost an infinite number of MOF structures can be designed due to the large variety of organic ligands and the rich coordination chemistry of metal centers [25].

The design of MOFs based photocatalysts for CO₂ reduction has been extensively researched and mainly targeted towards visible light responsive MOFs. This paper serves as a review of the advancements in MOF-based photocatalytic CO₂ reduction systems. It includes a comprehensive and analytical discussion of the recent developments in the design of photoactive MOFs and their application in photocatalytic CO₂ reduction. The article is divided into different sections: (i) MOFs as photocatalysts, with MOFs acting as both light harvesters and catalytic active sites; the ligand of the MOFs mainly absorbs the irradiated light; the photo-generated electrons from the ligands are transferred to the metal nodes to drive photocatalytic CO₂ reduction; (ii) MOFs as co-catalysts, involving the implementation of semiconductors to absorb the incident light, while MOFs act as support and co-catalyst; (iii) MOFs as hosts or catalytic scaffolds to support homogeneous catalytic centers, isolated metal sites, metal clusters and nanoparticles, in order to combine the best features of heterogeneous and homogeneous catalysts.

2. Main strategies for tuning the photocatalytic activity of MOFs

In the context of artificial photosynthesis, the flexibility and versatility of MOFs, as semiconductor materials, can provide a reaction platform inclusive of both light harvesters and active catalytic sites [45]. The presence of the organic ligand endows MOFs with their semiconductor behavior, by providing them with a broad light absorption band ascribed to a localized metal-to-ligand charge transition (MLCT), ligand-to-metal cluster charge transition (LCCT), or yet a π - π^* transition of the aromatic ligand, which has been proven to synergistically enhance photocatalytic reactions [46,47]. In this respect, organic ligands within MOFs primarily serve as light harvesters, which are excited upon light irradiation and generating the charge carriers. Subsequently, the mobile charge carriers activate the metal clusters to take part into heterogeneous photoredox reactions [48,49]. The semiconducting behavior of MOF-5, the first photocatalytic active MOF, was observed upon its exposure to light irradiation which resulted in charge separation decaying in a time scale of microseconds [46,50]. This initial success paved the way for the development of a series of semiconducting MOFs with good photocatalytic performance [51–54].

The numerous tunable metal centers and organic ligands in MOFs, combined with their unique porous structures, make them very promising semiconductor materials in photocatalysis [47]. The functionalization of MOFs is a method to enhance their photocatalytic activity. This can be pursued through the adjustment of the functional units that make up the MOF structure, such in the case of organic ligands manipulation to make them including reactive functional groups, or through the insertion of metal nodes with a higher reduction potential, or even a combination of both strategies [55]. MOF functionalization

can be carried out either via in-situ functionalization or post-synthetic modification (PSM). In the former approach, different functionalized ligands or metal clusters are directly used in the preparation of functionalized MOFs. On the other hand, PSM depends on the functionalization of synthesized parent MOFs with different metal oxides, heteropolyacids, amines, fluorescent dye quantum dots and others [56].

2.1. Adjusting organic ligands

The role of the organic ligands in the MOF structure is not only limited to framework structural stability, but extends to functioning as catalytic sites and light harvesters absorbing UV and visible wavelengths of sunlight [40]. In the MOF structure, organic ligands can trap the photons of appropriate wavelength; after that, functionalization of organic ligands or direct utilization of photoactive ligands provides them with the ability to modify both the wavelength and intensity of absorption [57].

2.1.1. Amine functionalized organic ligands

The first attempts at enhancing the photocatalytic activity of MOFs through functionalization of organic ligands were pioneered with the synthesis of NH₂-MIL-125 (Ti), through the introduction of an amino-functionalized organic ligand (H₂ATA) into the structure of MIL-125 (Ti) [58]. The presence of NH₂ in the organic ligand did not affect the structural stability of the parent MIL-125 (Ti); however, it led to an increase in its optical absorption, CO₂ adsorption and photocatalytic activity. Regarding optical absorption, the absorption band edge of the functionalized MOF extended to ca. 550 nm falling in the visible light region, compared to that of parent MIL-125 (Ti) at 350 nm, due to the influence of NH₂ groups on the charge transfer in the metal cluster. In terms of CO₂ adsorption, it was observed that the maximum CO₂ uptake in standard conditions for NH₂-MIL-125 (Ti) and parent MIL-125 (Ti) were 132.2 and 98.6 cm³ g⁻¹, respectively. The functionalization of the MOF's aromatic organic ligands with polar substitutes such as NH₂ enhanced its interaction with CO₂ molecules, through providing weak basic sites to interact with the acidic CO₂ [59]. Finally, regarding photocatalytic activity, it was observed that 10 h of visible light irradiation on NH₂-MIL-125 (Ti) generated 8.14 $\mu\text{mol HCOO}^-$, whereas the parent MIL-125 (Ti) was inactive under similar conditions (Fig. 2a). The high reactivity of NH₂-MIL-125 (Ti) was attributed to the functionalized ligand that facilitated the generation of separated excited charge states under visible light irradiation as shown in Fig. 2b. Subsequently, an electron was transferred from the excited organic ligand to Ti⁴⁺ in the metal cluster, leading to the formation of Ti³⁺, which consequently reduced CO₂ to HCOO⁻ in the presence of triethanolamine (TEOA) as electron donor. Interestingly, the reaction system was found inactive when benzyl alcohol was used as an electron donor under similar conditions, signifying the role of TEOA as an electron donor and its contribution to the adsorption of CO₂ owing to its more basic nature.

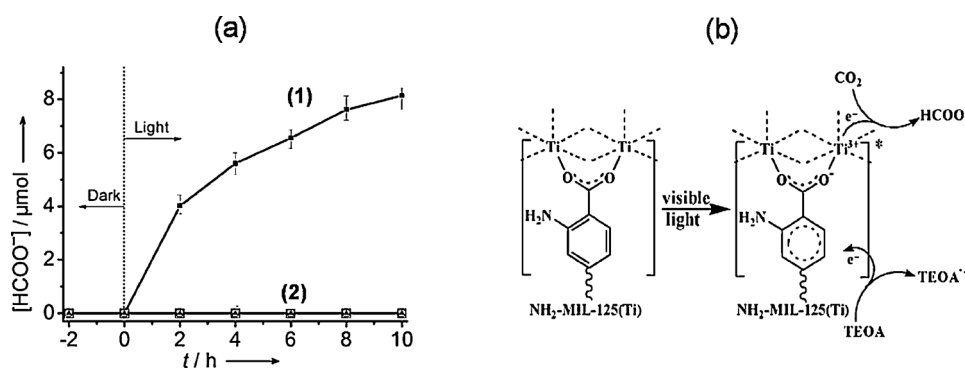


Fig. 2. (a) Generated HCOO⁻ as a function of irradiation time over (1) NH₂-MIL-125(Ti) and (2) MIL-125(Ti). (b) Proposed mechanism for the photocatalytic reduction of CO₂ over NH₂-MIL-125 (Ti) under visible light irradiation [58].

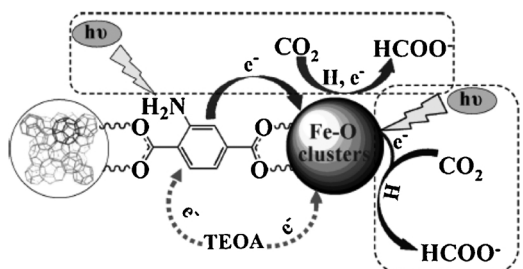


Fig. 3. Dual excitation pathways over amino functionalized Fe-based MOFs [61].

Assessing the origin of the carbon source in reaction products is of crucial importance as they may be formed from the degradation of the MOF structure rather than from CO_2 . To this end, carbon-13 nuclear magnetic resonance (^{13}C NMR) can be used to unambiguously demonstrate that the carbon source originates from CO_2 gas, thus confirming the selectivity of the tested MOF structure in converting CO_2 to the desired product. Indeed, it was observed that the product containing ^{12}C were corresponding only to the sacrificial agents (MeCN and TEOA), whereas other peaks were observed for the products obtained from the conversion of $^{13}\text{CO}_2$, which were assigned to the dissolved CO_2 , HCO_3^- and HCOO^- , hereby confirming that the produced HCOO^- originated from CO_2 as a reactant, and not from the photodegradation of the MOF structure.

Similarly, the photocatalytic activity of Uio-66 (Zr) was enhanced through amino-functionalized ligands using 2-aminoterephthalate (ATA) and 2,5-diaminoterephthalate (DTA) to produce a mixed-ligand MOF [60]. Similar to the findings of their previous work on MIL-125 [58], the presence of NH_2 group in the organic ligand using ATA in Uio-66 (Zr) structure, enhanced not only optical absorption, but also CO_2 adsorption capacity and the photocatalytic activity. It was observed that the concentration of HCOO^- produced over NH_2 -Uio-66 (Zr) increased with irradiation time, reaching $13.2 \mu\text{mol}$ after 10 h, and up to $25 \mu\text{mol}$ after 24 h, in contrast to the inactive parent MOF under similar conditions. This performance was further enhanced through the partial substitution of ATA with DTA in the organic ligand of NH_2 -Uio-66 (Zr) due to the additional NH_2 group in the mixed-ligand. It was observed that the addition of DTA expanded the light absorption edge to wavelengths greater than 500 nm compared to that of the parent NH_2 -Uio-66 (Zr) at 450 nm. Moreover, after 10 h under visible light irradiation, $20.7 \mu\text{mol}$ of HCOO^- were generated from the photocatalytic reduction of CO_2 using mixed-ligand NH_2 -Uio-66 (Zr) and reaching twice the amount acquired from the parent NH_2 -Uio-66 (Zr) after 24 h. This enhanced photocatalytic activity was attributed to the partial replacement of ATA with DTA in the MOF, and specifically to the additional NH_2 group of DTA.

The influence of amine functionalized organic ligand on the photocatalytic performance for CO_2 reduction over three typical Fe-based MOFs (MIL-101(Fe), MIL-53(Fe), and MIL-88B (Fe)) has also been investigated [61]. All of the chosen functionalized Fe-based MOFs have a similar organic ligand, 1,4-benzenedicarboxylate (BDC), but quite different structures due to the metal cluster. However, unlike the above mentioned NH_2 -free MIL-125 (Ti) and Uio-66 (Zr), in this occasion the parent MOFs exhibited a semiconducting behavior and were able to reduce CO_2 to formate under visible light irradiation. The amine functionalized Fe-based MOFs showed enhanced absorption in the visible light region extended to 700 nm along with a significantly enhanced CO_2 adsorption capability compared to the functionalized parent MOFs, due to the existence of the amine functionality as demonstrated by previous work. The Mott-Schottky method was applied to assess the semiconducting properties of MIL-101(Fe), the most reactive sample, upon light excitation. The flat band position was found to be -0.52 V vs NHE (normal hydrogen electrode), being more

negative than the reduction potential of CO_2 to form formate (-0.28 V vs NHE), indicating that the iron oxo clusters in MIL-101(Fe) can produce formate from CO_2 . Comparing the photocatalytic activity of the functionalized MOFs for the reduction of CO_2 to formate under visible light irradiation, it was found that all the MOFs functionalized with amine showed enhanced activity when the reaction system was compared to the corresponding parent MOF. After 8 h of visible light irradiation, the amount of HCOO^- formed over NH_2 -MIL-101(Fe), NH_2 -MIL-53(Fe), and NH_2 -MIL-88B (Fe) was $178 \mu\text{mol}$, $46.5 \mu\text{mol}$, and $30.0 \mu\text{mol}$, respectively. On the other hand, under similar conditions, the amount of formate produced over the parent MOFs for MIL-101(Fe), MIL-53(Fe), and MIL-88B (Fe) was $59.0 \mu\text{mol}$, $29.7 \mu\text{mol}$, and $9.0 \mu\text{mol}$, respectively. The different enhancement degree in the photocatalytic performance of the functionalized MOFs might have been related to the different efficiency of the electron transfer from the excited organic ligand to the metal center of these MOF materials. Nevertheless, the enhanced photocatalytic activity owing to the functionalized ligand was attributed to the formation of dual excitation pathways that played synergetic roles in the excitation of these functionalized Fe-based MOFs as shown in Fig. 3. The first pathway was credited to the visible light responsiveness of the parent Fe-based MOFs. Upon visible light irradiation, the excitation of the Fe-O cluster resulted in the transfer of an electron from O^{2-} to Fe^{3+} thus reducing Fe^{3+} to Fe^{2+} , which was capable of reducing CO_2 . It is worth nothing that the redox potential of the $\text{Fe}^{3+}/\text{Fe}^{2+}$ couple alone (0.77 V vs NHE) is not sufficient to reduce CO_2 , but that the final iron oxo clusters of the MOF can generate formate. The second excitation pathway was attributed to the amine functionalization of the organic ligand and involved the excitation of the NH_2 functional group followed by an electron transfer from the excited organic ligand to the metal center to generate Fe^{2+} , as previously observed for NH_2 -MIL-125(Ti) [58], and NH_2 -Uio-66(Zr) [60].

These works demonstrate that enhancing the photocatalytic activity of MOFs through the incorporation of amino groups into the organic ligand was an easy and effective strategy to extend the light absorption of MOFs [58,60,61]. This enhancement was due to the good chromophoric properties of amino groups to promote light harvesting of the ligand. Nevertheless, the extent of light absorption of these amine-functionalized MOFs is still not enough to fully utilize solar energy and should be further promoted. For example, the enhancement observed for NH_2 -MIL-125 (Ti) [58], and NH_2 -Uio-66 (Zr) and mixed ligand Uio-66 (Zr) [60], extended the absorption edge to 550, 450 and 500 nm, respectively. It is true that the absorption band fell within the visible light region and presented an enhancement in light absorption in contrast to the UV responsive parent MOFs. However, these materials did not exhibit any significant absorption at greater visible light wavelengths. On the other hand, the absorption edge of amino-functionalized Fe-based MOFs was extended to over 700 nm making them more effective in utilizing solar energy and the full spectrum of visible light.

Inspired by the fact that the increase of molecular conjugation degree can effectively enhance light absorption, the combination of conjugated molecules and amino groups is a feasible strategy to construct more photoactive organic ligands with a high light absorption capacity, which is in favor of upgrading MOF photoactivity [62]. An NH_2 -functionalized conjugated ligand ($\text{H}_2\text{SDCA-NH}_2$) was used in the synthesis of a Zr-based MOF, Zr-SDCA- NH_2 [63]. Both Zr-SDCA- NH_2 and $\text{H}_2\text{SDCA-NH}_2$ ligand presented a strong, consistent and broad absorption in the visible light range $400 \div 600 \text{ nm}$, demonstrating that the visible light responsiveness of the new MOF was basically originated from the modified ligand. The excellent light harvesting ability of $\text{H}_2\text{SDCA-NH}_2$ was due to the combined action between amino groups and the increasing conjugacy of the molecule. The higher light absorption band of $\text{H}_2\text{SDCA-NH}_2$ (600 nm) compared to non-amino modified H_2SDCA ligand (ca. 440 nm), and $\text{H}_2\text{DTA-NH}_2$ (ca. 550 nm) [60], gave evidence of the role of the chromophoric amino group and conjugacy of organic ligand in expanding the light absorption. The formate anion HCOO^- is the default product for CO_2 photoreduction in

acetonitrile when Zr-MOFs are employed as photocatalysts. TEOA is generally used in the reaction not only to provide an alkaline medium, but also to act as an electron donor and hydrogen donor to recycle the catalytic process in which the aldehyde form is its oxidative product [64]. The electronic structure of Zr-SDCA-NH₂ was investigated by Mott-Schottky measurements and it was found that the redox potential of LUMO and HOMO were -0.44 V and 1.83 V vs NHE, respectively. The more negative potential of LUMO than the reduction potential of CO₂ to formate is indicative of the ability of Zr-SDCA-NH₂ to photo-reduce CO₂ to formate. Moreover, the LUMO of H₂SDCA-NH₂ was -0.58 V vs NHE, suggesting that the ligand may also be active for CO₂ reduction. Regarding the photocatalytic activity, the evolved HCOO⁻ increased almost linearly with time under visible light irradiation when Zr-SDCA-NH₂ was used as a photocatalyst, reaching 18.8 μmol of HCOO⁻ after 12 h of irradiation. In contrast, 19.6 μmol of HCOO⁻ were generated when H₂SDCA-NH₂ was used. The photocatalytic active ligand compared to the inactive H₂ATA-NH₂ in NH₂-Uio-66 [60] demonstrated that the redox activity depends more on the structure of ligand rather than on the amino groups. Likewise to the reaction mechanism previously reported [64], a dual catalytic route exists in Zr-SDCA-NH₂ for CO₂ photoreduction reaction under visible light irradiation, where H₂SDCA-NH₂ ligand can serve as an antenna to absorb visible light for sensitizing metal clusters through the classical LCCT process, or it can be excited and directly reduce CO₂ to formate. These two catalytic routes increased the number of active sites in Zr-SDCA-NH₂, which may have contributed to its enhanced photocatalytic performance.

2.1.2. Porphyrin-based ligands

In natural photosynthesis, antenna light harvesting is done through porphyrin-like pigments. The highly conjugated, aromatic electron systems of porphyrins and metalloporphyrins are responsible for their chromophoric properties and photocatalytic activities [65]. In this context, an ordered MOF with porphyrin-based organic ligand might exhibit a similar behavior to that observed in natural photosynthesis. To this end, a porphyrin-based ligand (H₂TCP) was used in the direct synthesis of a Zr-based MOF, denoted as PCN-222, for effective CO₂ capture and photoreduction under visible light irradiation [66]. The synthesized MOF exhibited a broad light absorption band in the visible light region ($200 \div 800$ nm) owing to the incorporation of the photo-active H₂TCP ligand that behaved as an efficient visible light harvesting unit. Mott-Schottky measurements were performed on PCN-222 to evaluate its semiconductor character and ability of CO₂ reduction upon visible-light. The flat band position was determined to be -0.40 V vs. NHE, the LUMO was approximately equal to the flat band potential (-0.40 V vs. NHE), while the HOMO was 1.35 V vs NHE. Given the more negative potential of LUMO than the reduction potential of CO₂ to formate, it can be inferred that PCN-222 is able to photoreduce CO₂ to formate. In assessing PCN-222 photocatalytic activity for the reduction of CO₂ to formate, it was found that after 10 h of visible light irradiation (with TEOA as a sacrificial agent), 30 μmol of HCOO⁻ were generated, an amount significantly higher than that observed by the homogeneous reaction of the parent H₂TCP ligand (2.4 μmol of HCOO⁻) under similar conditions (Fig. 4 left). This enhanced photocatalytic activity of PCN-222 was due to the effective visible light absorption of H₂TCP ligand and the emergence of a unique and deep trap state that enabled the effective accumulation of long-lived photogenerated electrons readily available for the photocatalytic reduction of CO₂ molecules as confirmed by photoluminescence (PL) measurements. ¹³C NMR spectrum for products generated from using isotopic ¹³CO₂ in the above photocatalytic reaction gave an identifiable peak at 164.8 ppm corresponding to HCOO⁻, while no such signal was observed using ¹²CO₂ as shown in Fig. 4 right. These results confirmed that generation of formate was indeed from the reactant CO₂ and not from the photodegradation of the MOF structure, pointing to the stability of the MOF under the reaction conditions.

Similarly, H₂TCP was used as a ligand in the preparation of Zn/PMOF for the photocatalytic reduction of CO₂ to methane under visible light radiation in the presence of water as an electron donor [67]. In analogy with previously observed optical absorption change [66], the incorporation of H₂TCP ligand in Zn/PMOF resulted in broad absorption band in the visible light region ($300 \div 700$ nm); however, the absorption band exhibited a slight red shift when compared to the parent ligand. The photoreduction of CO₂ with H₂O into methane can proceed either through the formation of formaldehyde leading to the selective formation of methane or through carbene intermediates that lead to the formation of both methane and CH₃OH [68]. The formaldehyde path is the favorable one, where reaction conditions highly influence the dominating conversion pathway and the formed products. Moreover, the adsorption step on the catalyst surface at the beginning of the reactive process is a competition between CO₂ and H₂O molecules owing to the higher polar dipole moment exhibited by H₂O, resulting in a higher tendency to adsorb CO₂ [69]. Nonetheless, it was observed that after 4 h, 10.43 μmol CH₄ were produced using Zn/PMOF, on the other hand only 2.02 μmol CH₄ were generated using ZnO, while 0.52 μmol CH₄ were generated using TiO₂ under similar reaction conditions, indicating Zn/PMOF superior photocatalytic activity and high selectivity to the production of CH₄ through the formaldehyde pathway. However, photocatalytic deactivation of Zn/PMOF was observed after 4 h, which was postulated to be due to the partial saturation of the active sites with intermediate products, by-products, and CH₃OH formation. The adsorption of the latter has been detected during catalyst deactivation, indicating that the reaction at one stage proceeded through the carbene pathway. However, stable photocatalytic activity over three cycles along with confirmed stability from FTIR and UV/Vis absorption spectra after the reactions demonstrated the durability of Zn/PMOF under the reaction conditions.

2.1.3. Iridium-based and carboxylate ligands

The incorporation of photoactive functional units in MOF structures can make them more efficient light harvesters operating in the full range of visible light wavelengths for an effective exploitation of solar energy, thus rendering them more suitable for photocatalytic CO₂ reduction under visible light irradiation. For instance, Iridium (Ir) complexes are considered suitable in photocatalysis due to their broad visible light absorption from singlet-triplet transitions and the relatively long lifetime of the excited states [70]. To this end, a heterogeneous coordination polymer Ir-CP incorporating an Ir-based ligand was designed for the photocatalytic reduction of CO₂ to formate under visible light irradiation [71]. The addition of the Ir-based ligand that acted as an efficient light harvesting unit resulted in an extended absorption edge to 650 nm, due to enhanced metal to ligand and ligand to ligand charge transfer originating from the Ir-unit. As shown in Fig. 5a, after 6 h of visible light irradiation, 38.0 μmol of HCOO⁻ were obtained over Ir-CP, an output higher than that reported by previous works [58,60]. On the other hand, the homogenized parent Ir-unit generated 25 μmol of HCOO⁻ under similar conditions; however, it was rendered inactive after reaction due to its photodegradation, resulting in a drop of its light sensitizer efficiency. In contrast, Ir-CP exhibited high stability by remaining active with no noticeable change in the production of formate after multiple cycles, thus indicating that the incorporation of the Ir-unit in the coordination polymer did enhance not only its photocatalytic activity but also its stability and recyclability.

A carboxylate ligand H₂L, derived from an optically active chromophore of anthracene, was used in a Zr-based MOF, namely NNU-28, for the photocatalytic reduction of CO₂ to formate under visible light irradiation [64]. It was observed that NNU-28 exhibited a broad band visible light absorption up to 650 nm, due to the coordination between the metallic building units and ligand. The photocatalytic activity of NNU-28 for the photoreduction of CO₂ to formate under visible light irradiation exhibited a time-dependent increase in the concentration of HCOO⁻ under continuous visible light radiation. It was observed that

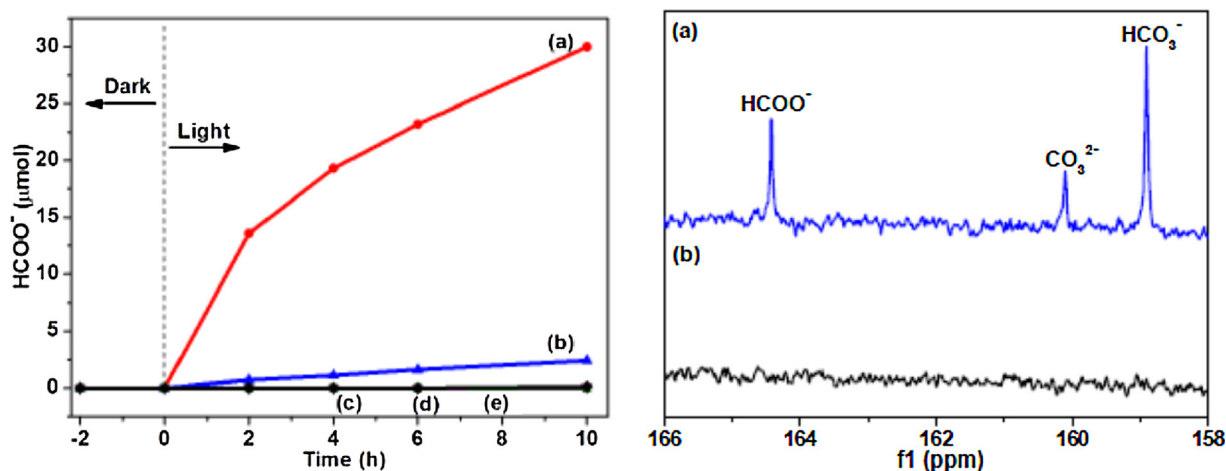


Fig. 4. Left: amount of HCOO^- produced under visible-light irradiation over (a) PCN-222, (b) H_2TCPP , (c) no PCN-222, (d) no TEOA, and (e) no CO_2 . Right: ^{13}C NMR spectra for the product obtained from the reaction with (a) $^{13}\text{CO}_2$ or (b) $^{12}\text{CO}_2$ [66].

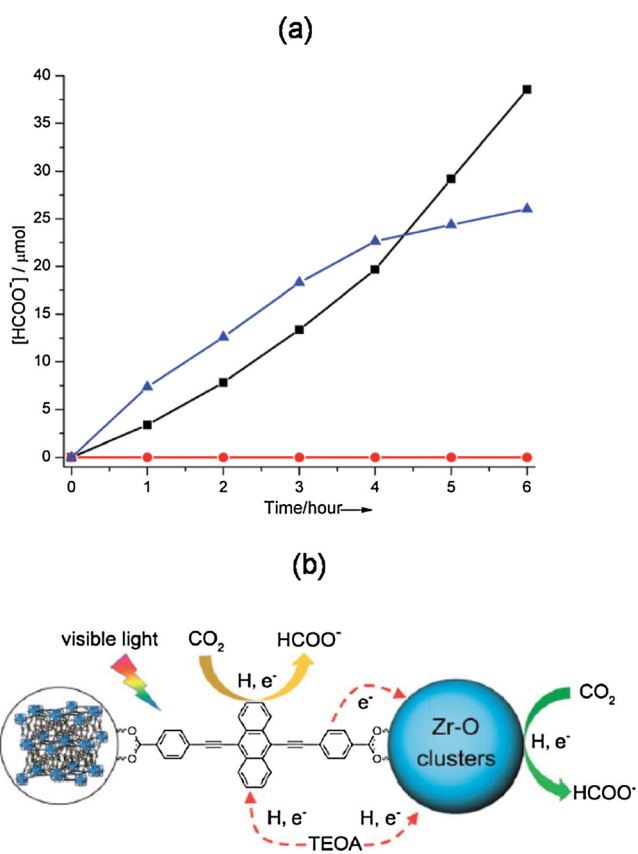


Fig. 5. (a) Produced HCOO^- using visible-light irradiation as a function of the time of radiation over microcrystals of Ir-CP (black curve with rectangular marker), without a sample (red curve with circle marker) and with Ir(ppy)₂(hdcbpy) in the homogeneous photocatalytic system (blue curve with triangle marker) [71]. (b) Schematic of dual photocatalytic routes for visible light driven CO_2 reduction in NNU-28 [64] (For interpretation of the references to colour in this figure legend, the reader is referred to the web version of this article.).

within 10 h, a total of 26.4 μmol of HCOO^- were generated, whereas under similar conditions 7.2 μmol of HCOO^- were produced over the anthracene-based ligand. This reactivity of the ligand indicated the existence of dual catalytic routes in NNU-28, due to both anthracene-based organic ligand and metal cluster (Fig. 5b). Upon visible light absorption, the anthracene-based ligand in NNU-28 not only acts as an

effective visible light harvester to the sensitized Zr_6 oxo cluster through the MLCT process, but also generates photoinduced charges by radical formation, thus resulting in the higher photocatalytic efficiency of NNU-28 compared to other Zr-based MOF structures.

2.2. Adjusting metal centers

Metal centers in the MOF structure are considered the primary sites for the catalytic activity of MOFs. The structure and mobility of metal clusters in MOFs have been extensively studied [72]. Transition metal ions are commonly used as inorganic clusters in the MOF structure, mainly due to their variety of coordination numbers and geometries giving rise to an endless variety of MOF structures [45]. In addition to changing organic ligands, another route to enhance visible light responsiveness and photocatalytic activity of MOFs can be through the functionalization of their metal centers.

The use of small iron (III) oxide clusters as inorganic nodes in MOFs has been previously investigated owing to their inherent absorbance of visible light; moreover, these clusters can be efficiently separated from each other due to confinement in a metal-organic framework. The incorporation of such iron oxides into MOF structure resulted in the formation of new MOFs such as MIL-100 (Fe) [73], amino-substituted MIL-101(Fe) [74], MIL-88B (Fe) [75], amino-substituted MIL-88B (Fe) [76], and Fe (III)-aminogel, an amorphous gel with a composition similar to amino-substituted MIL-101(Fe) [77]. Comparing the optical response of these photocatalytic materials using UV-vis spectroscopy in diffuse-reflectance mode has demonstrated that all of the as-prepared iron(III)-based solids have a clear optical response in the visible region in contrast to the UV active commercial titanium dioxide sample (P25) as shown in Fig. 6 [78].

Taking the semiconducting behavior of Fe-based MOFs into consideration, it can be concluded that they provide a valuable option in the photocatalytic reduction of CO_2 . This possibility was explored by using three Fe-based MOFs for the photocatalytic reduction of CO_2 reduction to formate under visible irradiation [61]. The chosen MOFs, MIL-101(Fe), MIL-53(Fe) and MIL-88B (Fe) all have the same organic ligand, yet with a different structure owing to the metal cluster: Fe_2O in MIL-101(Fe), FeO_6 octahedra in MIL-53 (Fe) and Fe_3O clusters in MIL-88B (Fe). All Fe-based MOFs exhibited a broad intense absorption band extending to the visible light region owing to the existence of large iron clusters in the structure that can lead to a red shift of the oxygen to iron charge transfer taking place in the visible region [79,80]. All three Fe-based MOFs exhibited quite a different CO_2 adsorption behavior: at the same conditions, MIL-101(Fe) showed the highest CO_2 adsorption capability with 26.4 g cm^{-3} , while over MIL-53(Fe) and MIL 88B(Fe)

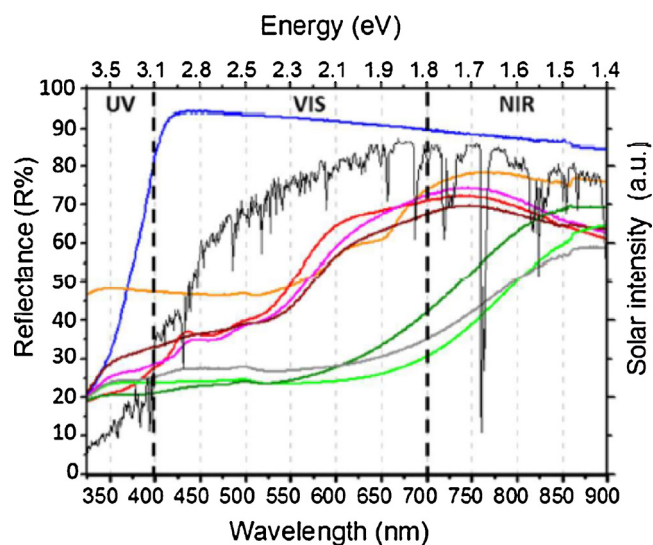


Fig. 6. Diffuse reflectance spectra of P25 (blue), Fe_2O_3 (gray), MIL-100(Fe) (orange), basolite F300 (red), MIL-88B (Fe) (pink), amino-substituted MIL-88B (Fe) (brown), amino-substituted MIL-101 (Fe) (light green) and Fe(III)-aminogel (green). The black curve represents solar spectrum (ASTM G173-03) [78] (For interpretation of the references to colour in this figure legend, the reader is referred to the web version of this article.)

adsorption extent was only 13.5 and 10.4 g cm^{-3} , respectively. The high adsorption capability of MIL-101(Fe) can be attributed to the direct adsorption of CO_2 onto the Fe center in the MOF since its structure contains unsaturated coordination Fe-metal sites (CUSs), the presence of which was confirmed by in-situ FTIR study. Under visible light irradiation for 8 h over all the three samples used to reduce CO_2 , it was observed that the generated HCOO^- over MIL-101(Fe), MIL-53(Fe), and MIL-88B(Fe) was 59 , 29.7 , and $9 \mu\text{mol}$, respectively. The generated amounts are higher than that obtained over conventional Fe_2O_3 ($5.6 \mu\text{mol}$ of HCOO^-). Although all three MOFs showed comparable visible light absorption, it was postulated that the significant photocatalytic activity of MIL-101 (Fe) originated from the direct adsorption of CO_2 onto the metal center due to the presence of unsaturated Fe metal sites, which is advantageous for the photocatalytic reduction of CO_2 . Moreover, electron spin resonance (ESR) studies confirmed that the iron-oxo cluster within the framework could directly reduce CO_2 to formate under visible light irradiation through a charge transfer from O^{2-} to Fe^{3+} , elucidating the role of the metal center (Fe) as a photocatalytic active site in MIL-101(Fe).

Copper metal complexes are well known for their activity towards CO_2 adsorption and photoreduction. Therefore their incorporation in MOFs might enhance CO_2 capture ability and photocatalytic activity [81,82]. Primarily, copper has good selectivity for photoreduction of CO_2 into methanol [83–85]. Based on this, a Cu-Porphyrin-based MOF photocatalyst (S_{Cu}) was synthesized for the photocatalytic CO_2 reduction and compared to its analogous MOF without Cu^{2+} (S_{p}) [86]. Both MOFs exhibited a strong absorption in the range $200 \div 800 \text{ nm}$, originating from the strong optical absorption behavior of the porphyrin-ligand; however, the introduction of copper into the structure resulted in a higher CO_2 adsorption capacity over S_{Cu} (277.4 mg g^{-1}), compared to that of S_{p} (153.1 mg g^{-1}). From the adsorption-desorption isotherms shown in Fig. 7a, it was inferred that S_{p} reversible desorption cycle was brought about by a physical interaction between CO_2 and S_{p} ; however, CO_2 was chemically adsorbed on S_{Cu} due to the irreversible desorption cycle as inferred from the open loop at 20 kPa . It was believed that the chemical adsorption of CO_2 on S_{Cu} was responsible for bending the linear CO_2 molecules, thus lowering the reaction energy barrier and improving S_{Cu} photocatalytic activity as demonstrated by the significantly higher methanol generation rate over S_{Cu} (262.6 ppm g^{-1}

h^{-1}) as compared to S_{p} ($37.5 \text{ ppm g}^{-1} \text{ h}^{-1}$) under visible light irradiation (Fig. 7b).

2.3. Mixed strategy

Enhancing the photocatalytic performance of semiconductors especially in the visible light region can be achieved through the introduction of metal-to-metal charge transfer (MMCT) by metal substitution to construct bimetallic assemblies. This is beneficial to photocatalysis as the bimetallic assemblies can harvest visible light, while the doped metal cation can act as an electron mediator to facilitate charge transfer [87–89]. This strategy has been previously applied on zeolites used for photocatalytic reduction of CO_2 , hydrogen evolution and alcohol oxidation [90,91]. Although bimetallic assemblies on semiconductors and zeolites have been shown to be promising for photocatalysis, the direct construction of bimetallic assemblies with a precise structure on these substrates is not straightforward. On the other hand, MOFs typically constituted of metal oxo-clusters interconnected by poly-dentate organic ligands, have a definite composition and structure. The partial substitution of metal cations in MOFs can lead to the formation of oxo-bridged hetero-metallic assemblies within the same MOFs [92,93]. Such bimetallic assemblies, similarly to those constructed over semiconductors and zeolites, are expected to show enhanced photocatalytic performance but with more flexibility and tunability due to the availability of different MOF structures.

The Zr-based MOF, UiO-66, cannot catalyze the reduction of CO_2 to HCOO^- , as the Zr_6 secondary building unit (SBU), namely $(\text{Zr}_6\text{O}_4(\text{OH})_4)$, cannot accept electrons from the BDC ligand under light irradiation because the redox potential energy level of the Zr_6 SBU in UiO-66 lies above the LUMO of the BDC ligands [94–97]. Consequently, it was hypothesized that embedding Ti ions into the Zr_6 SBU of UiO-66 trigger the catalytic activity of UiO-66 by lowering the redox potential energy of Zr_6 cluster. Post-synthetic exchange (PSE) was used to prepare Ti substituted NH_2 -UiO-66 (Zr), labeled as NH_2 -UiO-66 (Zr/Ti)-T-t, where T and t represent incubation temperature and time, respectively [98]. During MOF synthesis, it was found that the highest exchange of Zr by Ti moieties occurred with a treatment at $120 \text{ }^\circ\text{C}$ for 16 days, reaching a saturation amount in the as-obtained solid of about 57%, resulting in the formation of NH_2 -UiO-66 (Zr/Ti)-120-16. The electronic structures of undoped and Ti-doped NH_2 -UiO-66(Zr) were studied by DFT (density functional theory) calculations. The density of states and the band structure (Fig. 8a) of pure NH_2 -UiO-66(Zr) revealed that the valence band near the Fermi level can be mainly ascribed to the 2p states (lone pairs) of nitrogen atoms, whereas the bottom of the conduction band is mainly characterized by the p^* states of the ligand 2-aminoterephthalic acid (ATA), without the contributions of Zr atoms. Upon Ti introduction, new energy bands are evident in the conduction band of Ti-doped NH_2 -UiO-66(Zr) (Fig. 8b). The partial density of states (DOSs) of Zr and Ti atoms (Fig. 8c) showed that Ti atoms make significant contributions to the bottom of the conduction band of Ti-doped NH_2 -UiO-66(Zr), giving evidence of a favorable electron transfer from excited ATA to the Ti moiety to form $(\text{Ti}^{3+} / \text{Zr}^{4+})_6\text{O}_4(\text{OH})_4$ in Ti-doped NH_2 -UiO-66(Zr). The photocatalytic activity of NH_2 -UiO-66 (Zr/Ti)-120-16 was demonstrated for the reduction of CO_2 to HCOO^- under visible irradiation using TEOA as a sacrificial agent. It was observed that after 10 h, the HCOO^- produced over NH_2 -UiO-66 (Zr/Ti)-120-16 was $5.8 \text{ mmol mol}^{-1}$, while that generated over NH_2 -UiO-66 (Zr) was $3.4 \text{ mmol mol}^{-1}$ (Fig. 8d). The enhanced photocatalytic activity was due to the improved interfacial electron charge transfer from the excited ATA ligand to Zr-O oxo clusters promoted by the presence of the mediator Ti centers in the MOF structure as shown in Fig. 8e. Ti substitution led to the formation of $(\text{Ti}/\text{Zr})_6\text{O}_4(\text{OH})_4$, whereupon the excited ATA can transfer electrons to either Zr^{4+} or Ti^{4+} centers. As the presence of Ti atoms in the MOF structure contributed to the bottom of the conduction band, making the electron transfer from the excited ATA to the Ti moiety more favorable, the formation of the excited state

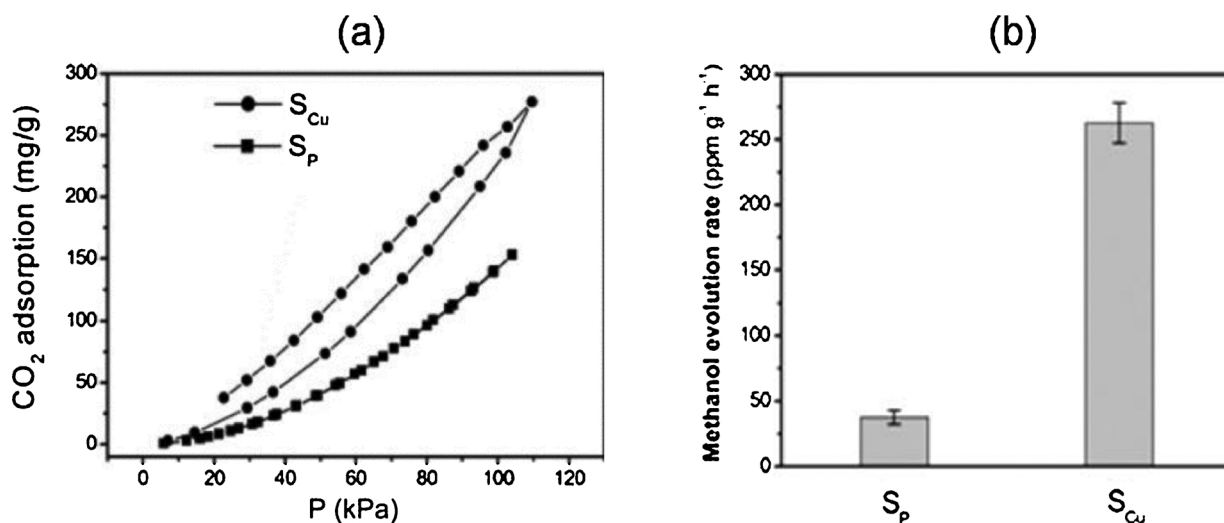


Fig. 7. (a) CO₂ adsorption and desorption isotherms of S_P and S_{Cu}; (b) methanol evolution rate over S_P and S_{Cu} [86].

(Ti³⁺/Zr⁴⁺)₆O₄(OH)₄ was expected. Subsequently, Ti³⁺ in the excited (Ti³⁺/Zr⁴⁺)₆O₄(OH)₄ can act as an electron donor to Zr⁴⁺ forming Ti⁴⁺-O-Zr³⁺.

In a more progressive effort, a mixed-ligand, mixed-metal UiO-66-derivative, denoted as 1(Zr/Ti), was prepared through PSE to carry out the photocatalytic CO₂ reduction to formate under visible light (Fig. 9) [99]. The introduction of a small amount of DTA as a co-ligand broadened the light absorption edge of the MOF. The mixed-ligand MOF was subjected to PSE to introduce Ti(IV) ions in the metal cluster, which in turn would become more capable of accepting electrons from the photoexcitation of the organic ligand. It was found that the ratios of Zr to Ti ions were 2.52 for 1(Zr/Ti) and 3.03 for UiO-66(Zr/Ti)-NH₂, which suggested that the Zr₆ metal clusters were converted to Zr_{4.3}Ti_{1.7} for 1(Zr/Ti) and Zr_{4.5}Ti_{1.5} for UiO-66(Zr/Ti)-NH₂. Turnover numbers (TONs) were calculated based on the Ti content, and it was found that, after 6 h of visible light irradiation, they were 6.27 ± 0.23 and 4.66 ± 0.17 for 1(Zr/Ti) and UiO-66(Zr/Ti)-NH₂, respectively.

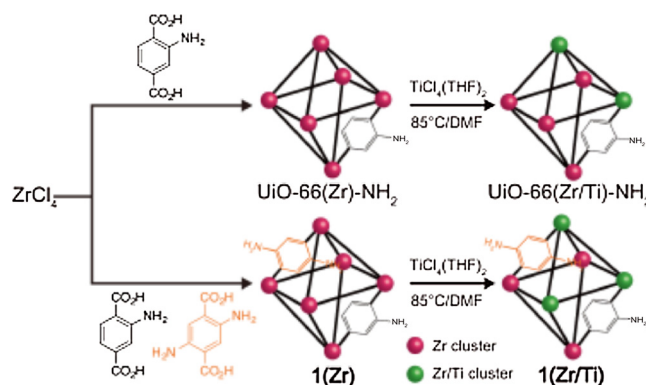


Fig. 9. Synthesis of mixed-ligand MOF 1(Zr) via post-synthetic exchange (PSE) to obtain mixed-metal MOFs 1(Zr/Ti), UiO-66(Zr/Ti)-NH₂ [99].

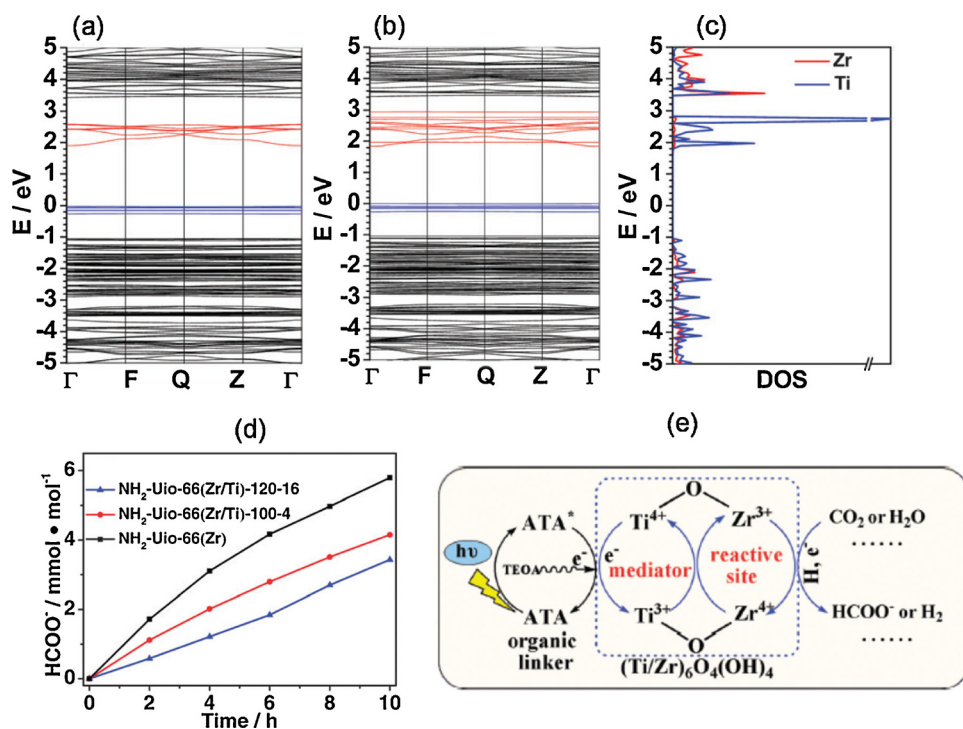


Fig. 8. (a) Band structure of NH₂-UiO-66(Zr). (b) Band structure of Ti-doped NH₂-UiO-66(Zr). (c) Partial density of states (DOS) of Zr and Ti atoms in the Ti-doped NH₂-UiO-66(Zr). (d) HCOO⁻ production as a function of irradiation time over different samples. (e) Proposed mechanism for the photocatalytic reactions over NH₂-UiO-66 (Zr/Ti). In parts (a–c), the Fermi level is set to zero [98].

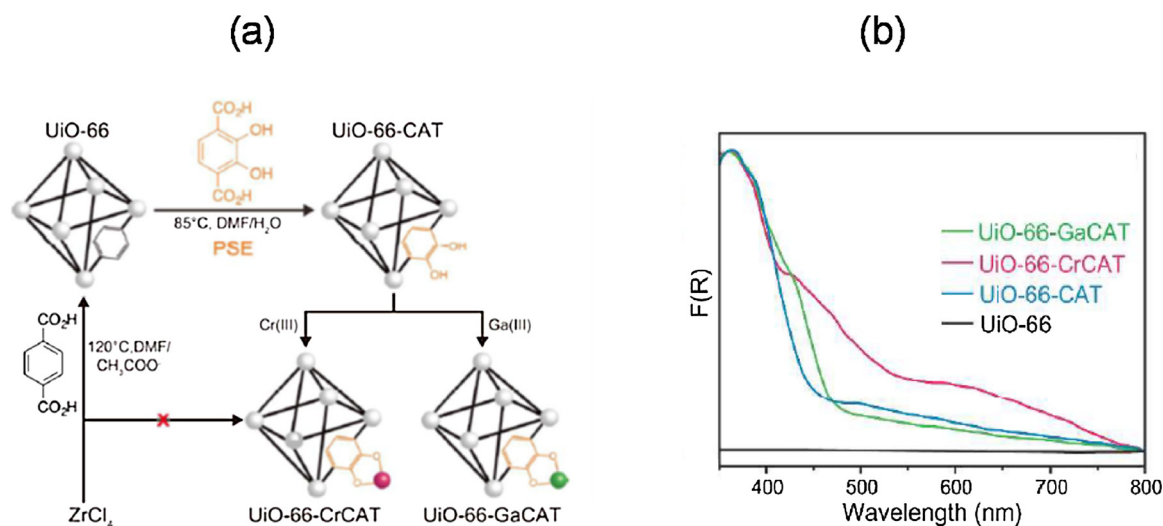


Fig. 10. (a) Preparation of MOF photocatalysts through post-synthetic exchange (PSE) and metalation. (b) UV/Vis diffuse reflectance of UiO-66, UiO-66CAT, UiO-66CrCAT, and UiO-66-GaCAT [100].

However, using the parent MOFs, 1(Zr) and UiO-66(Zr)-NH₂, did not result in the generation of HCOOH indicating the role of Ti clusters in promoting the photocatalytic activity of these MOF structures.

The incorporation of other catalytic metal sites into MOF photocatalysts through PSE for CO₂ reduction was explored by Cohen and coworkers [100]. The starting MOF, UiO-66 (Zr) was subjected to PSE with a catechol-functionalized organic ligand (catbdc), to produce UiO-66-CAT. Subsequently, Cr (III) and Ga (III) were incorporated into the (catbdc) sites to produce M (III)-monocatecholato functionalized MOFs as shown in Fig. 10a. Through this strategy, the catbdc organic ligands would be responsible for visible light absorption, while metalation by Cr (III) and Ga (III) would facilitate electron transfer within the MOFs. PSE and metalation of the designed MOFs changed their light absorption edges as demonstrated by UV/Vis spectroscopy shown in Fig. 10b, resulting in higher absorption edges of all modified MOFs compared to the parent UiO-66 (Zr). The introduction of the catechol groups was responsible for the better visible light absorption of UiO-66-CAT compared to UiO-66 (Zr). Moreover, UiO-66-CrCAT demonstrated the highest light responsiveness due to LCCT induced by Cr (III) binding to (catbdc) sites. It was found that after 6 h of visible light irradiation, 51.73 μmoles HCOO⁻ were generated over UiO-66-CrCAT, almost twice as much as those generated over UiO-66-GaCAT (28.78 μmol HCOO⁻). This higher photocatalytic activity was due to the more suitable reduction potential of Cr(III) for CO₂ reduction, along with UiO-66-CrCAT's more effective charge transfer as corroborated through photoluminescence spectroscopy results. On the other hand, UiO-66-CAT was inactive as a photocatalyst under similar conditions, indicating that the metalation of the MOF was responsible for its photocatalytic activity.

3. MOFs as co-catalysts

In many cases, a performance deficit exists in the case of photocatalytic application of MOFs when compared to their inorganic semiconductor counterparts. This can be ascribed to MOFs low efficiency in generating excited states and ensure charge separation [101]. A possible solution to this problem is the integration of an enhanced CO₂ adsorption ability into the MOF structure, on one hand, with an excellent exciton generation achieved via an inorganic semiconductor, on the other. It is believed that this approach boosts the efficiency of photocatalytic reactions in the gas phase (i.e. CO₂ reduction). However, the success of this approach is dependent on the effective photoexcited electron transfer from the semiconductor to the MOF structure [102].

3.1. Coupling with transition-metal-based semiconductor photocatalysts

A hybrid catalyst in a core-shell configuration, namely Cu₃(BTC)₂@TiO₂, was designed for the photocatalytic reduction of CO₂ to CH₄ with the aid of water [102]. Notably, no organic sacrificial electron donor was used in this work. Within this hybrid catalysts, the MOF based core Cu₃(BTC)₂ (BTC: benzene-1,3,5-tricarboxylate) provided a large surface area for the adsorption and photoconversion of CO₂, while the outer TiO₂ shell acted as a semiconductor for the photocatalytic conversion of CO₂. TiO₂ was formulated as a macro-porous shell to be easily photoexcited and to facilitate the diffusion and capture of gas molecules in the MOF based core.

N₂ adsorption and desorption isotherms demonstrated that the total surface area of bare Cu₃(BTC)₂ of 1183 m² g⁻¹ was higher than that of Cu₃(BTC)₂@TiO₂, which was 756 m² g⁻¹. This decrease was attributed to the presence of the small surface area TiO₂ shells that took a third of the total weight. The obtained Type I adsorption-desorption curves indicated the micro-porosity of Cu₃(BTC)₂. Moreover, Cu₃(BTC)₂@TiO₂ core-shell demonstrated a similar trend with a slight hysteresis in the desorption curve, indicating that the Cu₃(BTC)₂ core contributed to micro-porosity, while TiO₂ shell contributed to meso- and macro-porosity. On the other hand, CO₂ adsorption uptake on Cu₃(BTC)₂ and Cu₃(BTC)₂@TiO₂ core-shell amounted to 80.75 and 49.17 cm³ g⁻¹, respectively, based on total sample weight. The decrease in CO₂ uptake for Cu₃(BTC)₂@TiO₂ core-shell was accounted for by the weight of TiO₂, as seen from the N₂ isotherms. Nevertheless, CO₂ uptake for Cu₃(BTC)₂ in the hybrid catalyst structure was 73.75 cm³ g⁻¹, which was comparable to that of Cu₃(BTC)₂, indicating that the CO₂ molecule can pass through the macro-porous TiO₂ shell and be adsorbed on the micro-porous Cu₃(BTC)₂ core.

Regarding the photocatalytic activity of the developed hybrid structure for the conversion of CO₂ to CH₄ under UV illumination, it was found that the yield in CH₄ using Cu₃(BTC)₂@TiO₂ core-shell was five times higher than that obtained with bare TiO₂ nano-crystals, as shown in Fig. 11a. Moreover, the CH₄ selectivity compared to other products (particularly H₂) was significantly higher with Cu₃(BTC)₂@TiO₂ core-shell than that observed with pure TiO₂ nano-crystals owing to the presence of the Cu sites in the MOF based core, along with the higher electron density originating from the improved electron-hole separation in the hybrid structure. Regarding the reaction mechanism, it was hypothesized that TiO₂ in the hybrid structure is photoexcited to generate electron-hole pairs and the electrons are transferred to the Cu₃(BTC)₂ core. Subsequently, CO₂ reduction takes

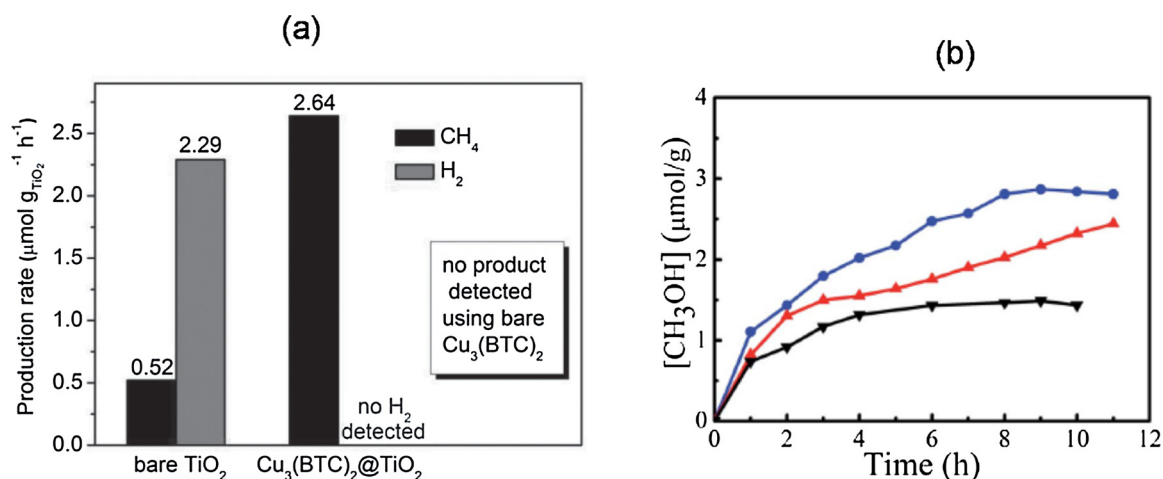


Fig. 11. (a) Production yields of CH₄ and H₂ from CO₂ over bare TiO₂ nanocrystals and Cu₃(BTC)₂@TiO₂ core-shell under UV irradiation for 4 h [102]. (b) CH₃OH generation over Zn₂GeO₄ nanorods (black curve), Zn₂GeO₄/ZIF-8 nanorods (red curve), and Pt-loaded Zn₂GeO₄/ZIF-8 nanorods (blue curve) as a function of light irradiation time [103] (For interpretation of the references to colour in this figure legend, the reader is referred to the web version of this article.).

place on the Cu sites of Cu₃(BTC)₂, where the gas molecules can be adsorbed, while the oxidation occurs on TiO₂ surface.

A semiconductor-MOF nano-composite was synthesized by growing ZIF-8 nanoparticles on Zn₂GeO₄ semiconductor nano-rods for the photocatalytic conversion of CO₂ into CH₃OH [103]. Photocatalytic reduction of CO₂ to methanol in aqueous solution was performed over Zn₂GeO₄ and Zn₂GeO₄/ZIF-8. Upon light irradiation for 10 h over Zn₂GeO₄ nano-rods, 1.43 μmol g⁻¹ of CH₃OH were generated. On the other hand, under similar conditions, using Zn₂GeO₄/ZIF-8 resulted in the formation of 2.44 μmol g⁻¹ of CH₃OH, which kept on increasing with irradiation time. The 62% increase in reaction yield over Zn₂GeO₄/ZIF-8 compared to Zn₂GeO₄ was due to the introduction of ZIF-8, which can effectively adsorb dissolved CO₂ in water solution along with its contribution to enhanced light absorption. The rate of CH₃OH generation was further enhanced by loading Pt as a co-catalyst, aiming to improve the separation of photogenerated electron-hole pairs (Fig. 11b).

An innovative hybrid photocatalyst was designed by coupling UiO-66-NH₂ with Cd_{0.2}Zn_{0.8}S semiconductor for the photocatalytic H₂-production and CO₂ reduction [104]. UV-vis spectra showed that the incorporation of Cd_{0.2}Zn_{0.8}S into UiO-66-NH₂ resulted in a slight red shift, with absorption edges of longer wavelengths compared to Cd_{0.2}Zn_{0.8}S and UiO-66-NH₂, suggesting that the composites can absorb more visible light. Moreover, in terms of N₂ adsorption isotherms, all Cd_{0.2}Zn_{0.8}S@UiO-66-NH₂ samples exhibited hybrid type I/IV isotherms with a large hysteresis between adsorption and desorption branches, revealing the presence of a combination of micropores from UiO-66-NH₂ and mesopores from Cd_{0.2}Zn_{0.8}S.

The photocatalytic activity of the Cd_{0.2}Zn_{0.8}S@UiO-66-NH₂ composites was evaluated by using them in the photoreduction of CO₂ dissolved in NaOH solutions under visible-light irradiation (Fig. 12a). All the Cd_{0.2}Zn_{0.8}S@UiO-66-NH₂ samples exhibited superior photocatalytic activity as compared to the bare Cd_{0.2}Zn_{0.8}S, and UiO-66-NH₂ content had a significant influence on the photocatalytic activity. Among the as-prepared samples, CZS@UN20 (20 wt% UiO-66-NH₂) presented the highest CH₃OH evolution amount of 6.8 μmol h⁻¹ g⁻¹ during visible-light irradiation, which was 3.4 times higher than that obtained over pure Cd_{0.2}Zn_{0.8}S. The corresponding photocatalytic mechanisms for H₂ production and CO₂ reduction are depicted in Fig. 12b. Visible-light irradiation led to the excitation of UiO-66-NH₂ and Cd_{0.2}Zn_{0.8}S, followed by generation of electron-hole pairs. The photoinduced electrons on the LUMO of UiO-66-NH₂ can hence directly transfer to the CB of Cd_{0.2}Zn_{0.8}S, inhibiting the recombination of generated electron-hole pairs and prolonging their lifetime. After that, OH

is produced from the oxidation of H₂O by the generated holes, releasing O₂ and H⁺; CH₃OH is thus formed from CO₂, H⁺, and the excited electrons.

3.2. Co-ZIF-9: an example of a hybrid photochemical system

In a series of works, Wang and coworkers synthesized a microporous co-catalyst based MOF, named Co-ZIF-9 and formed by cobalt (III) linked to benzimidazolone (blm) ligands, which was employed for the visible light induced photocatalytic reduction of CO₂ to CO in the presence of a photosensitizer [105–107]. Their first attempt involved the use of a Ru-based photosensitizer combined with the catalyst mentioned above [105]. It was observed that, under visible light radiation, the photocatalytic reaction in the presence of Co-ZIF-9 and the photosensitizer led to the formation of 41.8 μmol CO and 29.9 μmol of H₂. On the other hand, in the absence of Co-ZIF-9, the production rate of CO and H₂ decreased substantially to 1.2 and 1.8 μmol, respectively, highlighting the role of the co-catalyst in promoting the photocatalytic activity of the reaction system. One of the main issues posed by this system is the instability of the Ru-based photosensitizer, which drastically reduces its performance over time.

The risk of instability of such hybrid systems has been overcome by the use of a metal-free conjugated carbon nitride polymer semiconductor (g-C₃N₄) as a mesoporous photocatalyst, in conjunction with Co-ZIF-9 as a microporous crystalline co-catalyst and bipyridine (bpy) as an auxiliary electron mediator for the previously mentioned reactive system [106]. Exposure to visible light (> 420 nm) for 2 h resulted in the production of 20.8 μmol of CO from the photocatalytic reduction of CO₂, along with the generation of 3.3 μmol of H₂. Regarding the stability, it was revealed that this reaction system kept its original catalytic activity almost unaffected after seven cycles with a catalytic TON of 35 with respect to Co-ZIF-9 (Fig. 13a). In the optimal reaction conditions, the apparent quantum yield of this hybrid system was 0.9% under monochromatic irradiation of 420 nm. FTIR and XRD characterizations run on the used Co-ZIF-9 and g-C₃N₄ showed no apparent changes in the chemical and crystal structures of Co-ZIF-9 and g-C₃N₄, reflecting their stability during the photocatalytic reaction.

In another attempt, CdS was also used as a semiconductor for the same reaction system [107]. The catalytic activity was investigated under various reaction conditions. After 1 h of visible light irradiation, the catalytic system resulted in the generation of 50.4 μmol of CO and 11.1 μmol of H₂. The generation rate of both products increased linearly with reaction time, with the concentration of CO and H₂ reaching 85.6 μmol and 38.8 μmol, respectively, after 3 h of irradiation

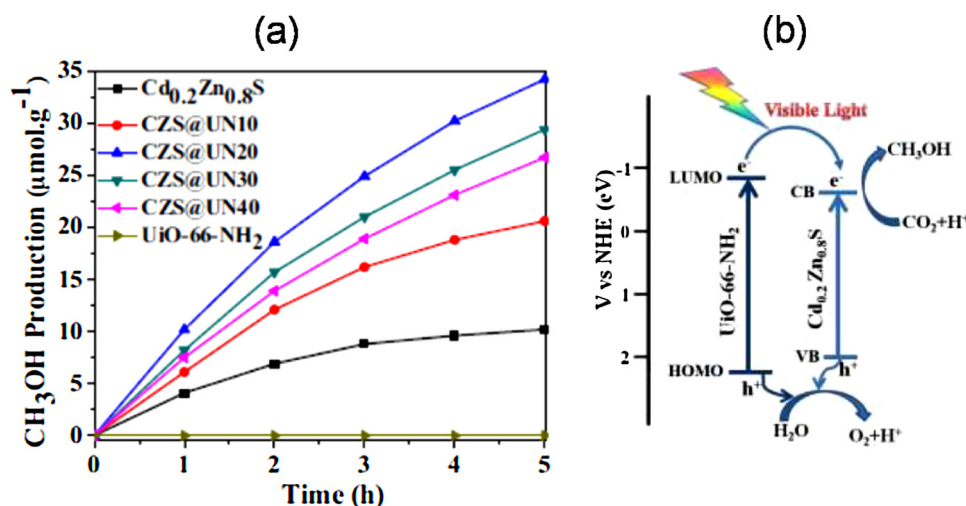


Fig. 12. (a) CH₃OH generation over various Cd_{0.2}Zn_{0.8}S@UiO-66-NH₂ composites vs. irradiation time. (b) Schematic of the photogenerated electrons and holes transfer in the Cd_{0.2}Zn_{0.8}S@UiO-66-NH₂ composite and mechanism of the photocatalytic CO₂ reduction under visible light irradiation.

(Fig. 13b). In the optimal reaction conditions, an apparent quantum yield of 1.93% by monochromatic irradiation at 420 nm was achieved for the photochemical system. However, the rate of production after 1 h started to gradually diminish due to the chemical instability of the CdS semiconductor and the depletion/degradation of CO₂ and bpy after long time operations under the reaction conditions. Nevertheless, the Co-ZIF-9 co-catalyst was able to preserve its intrinsic catalytic activity, which had been previously confirmed [105,106]. A possible reaction mechanism for the CO₂ photocatalytic reduction system was proposed,

where upon visible light irradiation the electron-hole pairs were generated on the CdS semiconductor, as shown in Fig. 13c. The visible light-excited electrons migrated to the conduction band of CdS and, subsequently, were transferred to Co-ZIF-9, to interact with the adsorbed CO₂ molecules, eventually affording CO via CO₂^{-•} (stabilized by the benzimidazole linkers in Co-ZIF-9). At the same time, protons present in the reaction system were directly reduced by the excited electrons, thus forming H₂. The generated holes were quenched by TEOA acting as the sacrificial electron donor.

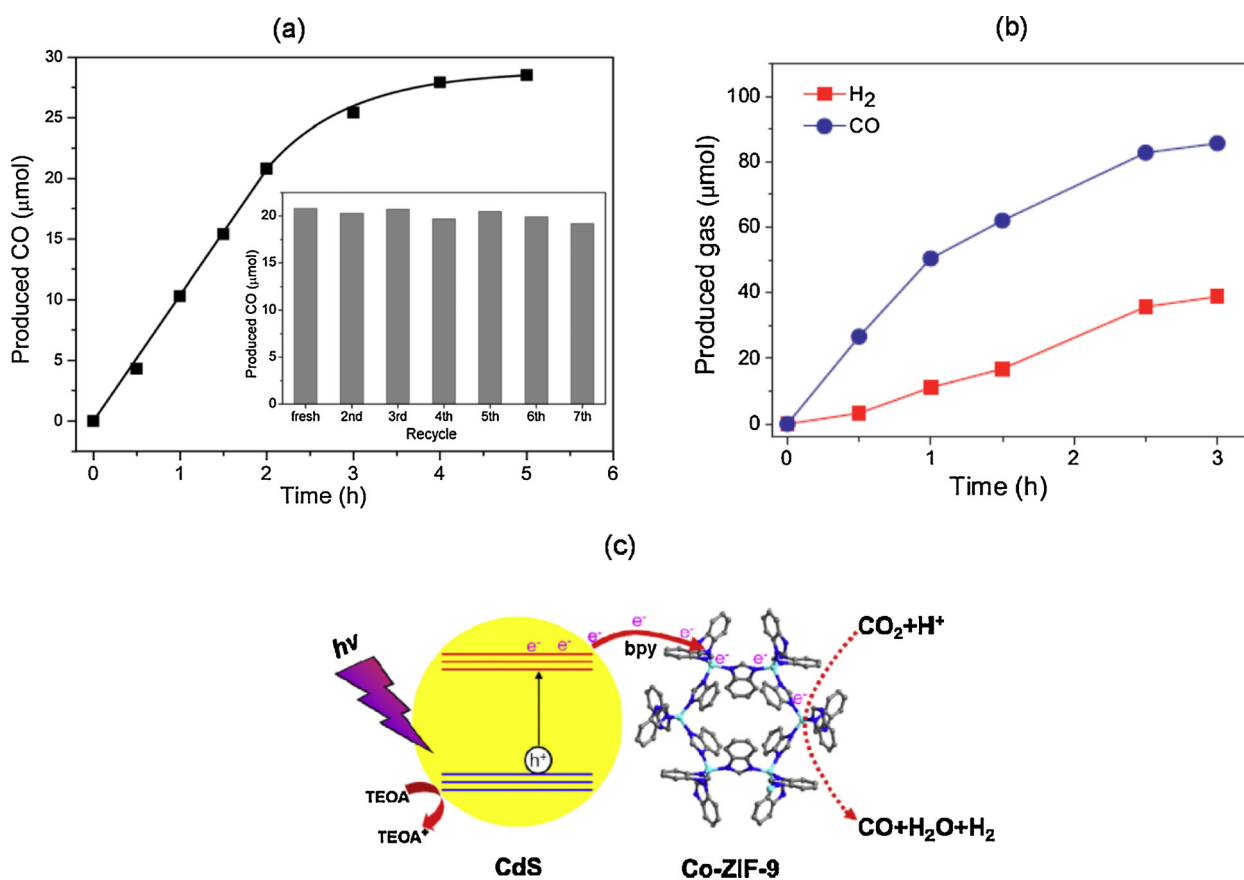


Fig. 13. (a) CO production from the CO-ZIF-9 catalyzed CO₂ conversion systems as a function of the reaction time. Inset: a stability test of the CO₂ photoreduction system for seven repeated operations [106]. (b) Production of CO and H₂ from the Co-ZIF-9 and CdS co-catalyzed CO₂ photoreduction system under visible illumination [107]. (c) Possible reaction mechanism for the Co-ZIF-9 co-catalyzed photoreduction of CO₂ employing CdS as light harvester [107].

4. MOFs as hosts and sacrificial precursors

A strategy different from the ones reported in the previous sections consists on utilizing MOFs as hosts or sacrificial precursors. In such case, MOFs have no or weak catalytic activity in the photochemical reactions, and they are only used as materials to support catalysts. Isolated metal sites, metal clusters, and nanoparticles are incorporated into the structure, with the resultant MOF-based composites exhibiting an enhanced performance for light-induced reactions. The motivation for utilizing MOFs as catalytic scaffolds lay in their potential to combine the best features of heterogeneous and homogeneous catalysts. Being solid-state materials, MOFs afford good thermal stability and can be easily separated from substrates and products in gas and liquid phases. Also, they have the ability to be chemically tuned to the same level as a homogenous molecular catalyst. Consequently, MOFs have been served as heterogeneous platforms to immobilize a great variety of functional moieties like organometallic catalysts, nanoparticles, polyalkyl amine chains, and enzymes [108].

A rhodium-based catalytic system for CO₂ reduction has been recently developed using this strategy [109]. Such catalyst used UiO-67 MOF as an immobilization platform for Cp*Rh(bpydc)Cl₂ (bpydc = 2,2'-bipyridine-5,5'-dicarboxylic acid) molecular complex through post-synthetic exchange, yielding a rhodium-functionalized UiO-67, namely Cp*Rh@UiO-67. The bdc- ligands were replaced with the rhodium-based molecular complex at 5, 10, 20 and 35%. Photocatalytic conversion of CO₂ to formate was performed using 10%-Cp*Rh@UiO-67 with TEOA as an electron donor, and in the presence of [Ru(bpy)₃Cl₂, bpy = 2,2'-bipyridine] as a photosensitizer (Fig. 14a). It was found that after 10 h of visible light irradiation, the modified MOF gave a formate TON of 47, which was higher than that obtained through its parent homogenous molecular complex, which was 42. On the other hand, the TON for H₂ from the modified MOF was 36, lower than that obtained by its analogues molecular complex with TON of 38. The overall stability of both systems was comparable and the loss of activity during the catalytic reaction was attributed to the decomposition of the photosensitizer over several hours. Considering the effect of increasing the amount of rhodium in Cp*Rh@UiO-67 on the initial formation rates of formate and H₂, it was found that a plateau is reached above a 10% Rh incorporation into the UiO-67 framework, whereas increasing the Rh-loading between 5%- and 10% doubled the production rates of formate and H₂ as shown in Fig. 14b. Beyond 10% Rh incorporation, the H₂/formate ratio increased by increasing rhodium loading, with the formate production decreasing by approximately the same amount by which H₂ production was enhanced. This led to the conclusion that the 10% Rh in Cp*Rh@UiO-67 was the optimal balance between CO₂ reduction to formate and formate decomposition to H₂. Below this point, the good accessibility of the external photosensitizer to the catalytic

sites owing to the limited Rh incorporation might favor CO₂ reduction by Rh centers. On the other hand, increasing the percentage incorporation above 10% will reduce available porosity, inhibiting the access of the photosensitizer and favoring thermal decomposition of formate by the rhodium centers.

Further relevant work in this area was performed on a manganese bipyridine which was incorporated into a Zr(IV)-based MOF with open bpy metal-chelating linkers [110]. This was subject to post-synthetic metalation to achieve isolated Mn(bpy)(CO)₃Br moieties in the MOF structure, forming UiO-67-Mn(bpy)(CO)₃Br. The synthesized catalyst was utilized for the photocatalytic reduction of CO₂ to formate in the presence of [Ru(dmb)₃]²⁺ (dmb = 4,4'-dimethyl-2,2'-bipyridine) as a photosensitizer and BNAH as a sacrificial agent. It was found that roughly 76% of bpy sites were metalated and increasing bpy sites functionalization beyond this point did not enhance the incorporation of Mn(bpy)(CO)₃Br moieties due to steric hindrance by the Mn-complexes in the MOF cavities.

The photocatalytic reduction of CO₂ over the designed UiO-67-Mn(bpy)(CO)₃Br was highly selective to formate production, by which formate TONs were 50 and 110 over 4 and 18 h, respectively. The resulting photocatalytic activity was higher than its homogeneous analogues, namely Mn(bpy)(CO)₃Br and Mn(bpydc)(CO)₃Br, along with a mixture of the homogeneous Mn(bpy)(CO)₃Br complexes in combination with UiO-67, as shown in Fig. 15a. This highlighted the role of the framework of UiO-67-Mn(bpy)(CO)₃Br in stabilizing the Mn(CO)₃ moiety and inhibiting dimerization in the singly reduced Mn-complex. Furthermore, the MOF structure could act as a source for supplying CO₂ to the Mn active sites due to their high CO₂ adsorption ability. However, catalyst recyclability studies pointed to a loss in the photocatalytic performance over three cycles due to the degradation of the MOF framework and loss of the Mn(CO)₃ moiety, by which CO ligands were lost from the Mn catalytic sites in the framework, resulting from prolonged visible light irradiation and exposure to the alkaline solution. According to the hypothesized mechanism, the photocatalytic reaction is initiated by the reduction of the excited photosensitizer by BNAH. An electron is then transferred from the reduced photosensitizer to the Mn-complex, forming an Mn(0) complex; this is facilitated by the large pores of UiO-67 allowing for electron transfer between the photosensitizer and the Mn-complex within the MOF. Subsequently, TEOA donates one proton and one electron to the catalytic reaction, forming a Mn(I)-H complex, to which CO₂ molecule can bind, forming a Mn(I)-OC(O)H complex. Then, formate is produced from the dissociation of the latter, eventually regenerating the starting Mn(I) complex as shown in Fig. 15b.

The strategy of using MOFs as sacrificial precursors can also be effective to achieve better control regarding phase, shape, morphology, and synthesis of nanoparticles [111]. To this aim, NH₂-MIL-125(Ti) MOF was employed as a sacrificial precursor to synthesize TiO₂

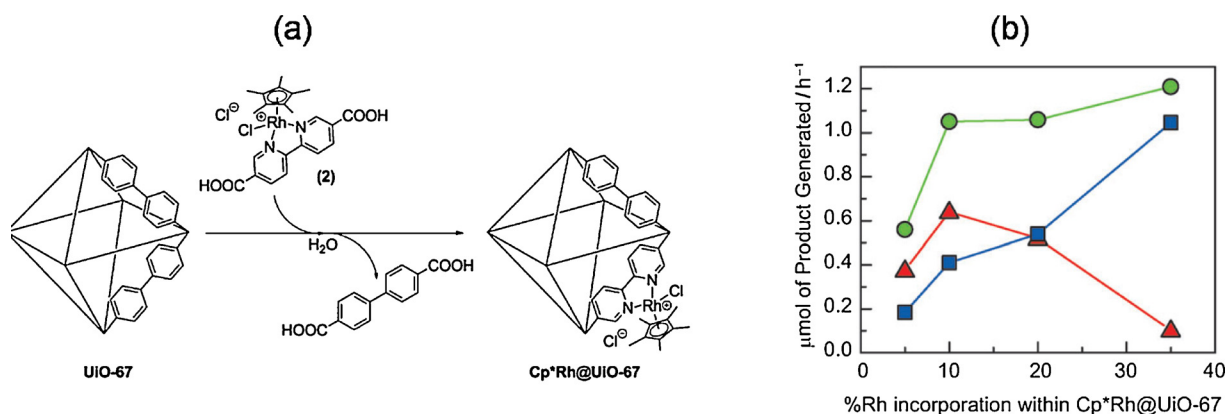


Fig. 14. (a) Heterogenization of a rhodium complex into the framework of UiO-67 through post-synthetic linker exchange. (b) Effect of rhodium catalyst loading on the production of formate (red curve), H₂ (blue curve), and their sum (green curve) for the heterogeneous 10%-Cp*Rh@UiO-67 (For interpretation of the references to colour in this figure legend, the reader is referred to the web version of this article.).

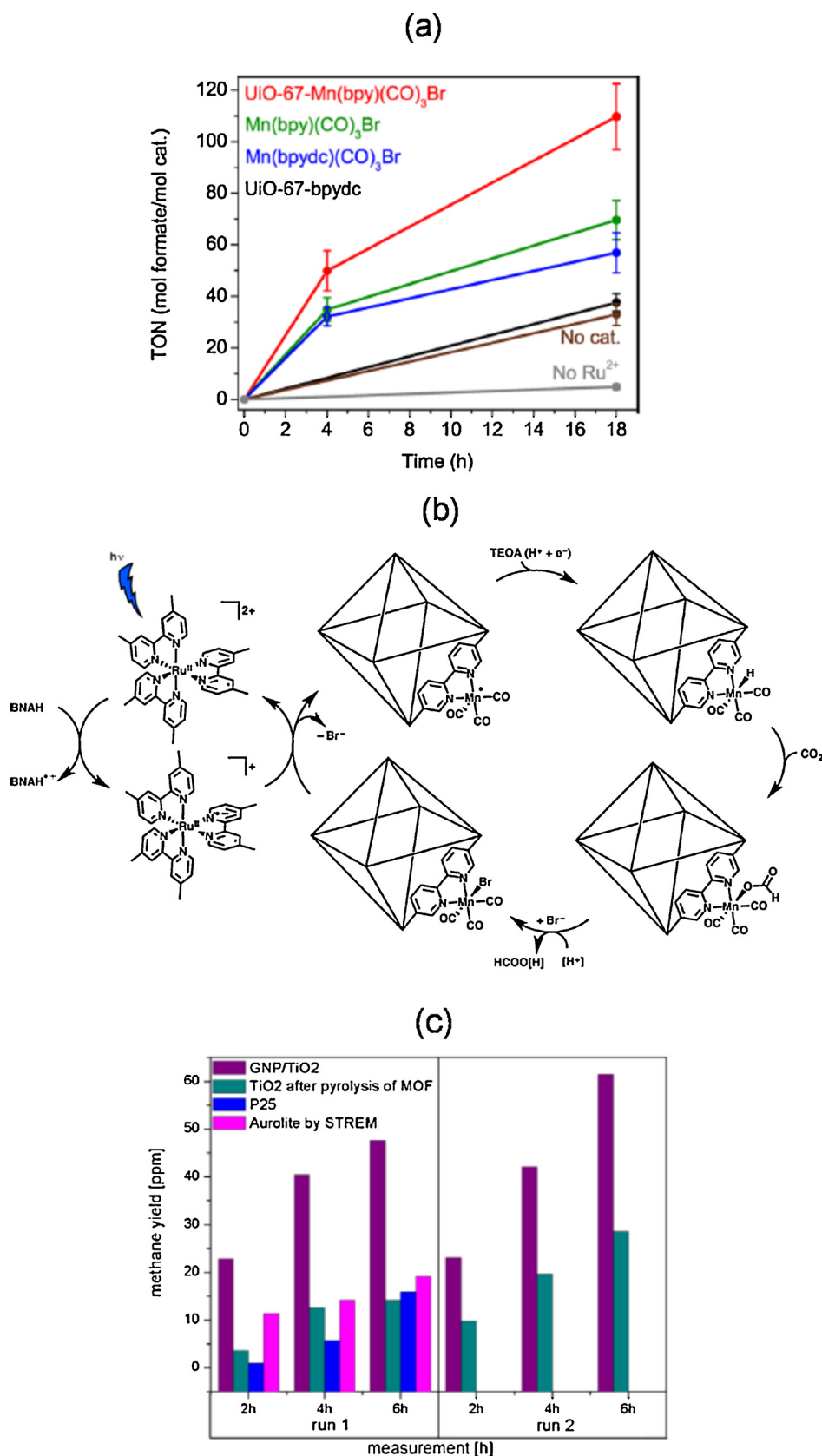


Fig. 15. (a) Formate turnover number (TON, mol of formate / mol of catalyst) during photocatalysis experiments for UiO-67-Mn(bpy)(CO)₃Br, Mn(bpy)(CO)₃Br, Mn(bpydc)(CO)₃Br, UiO-67-bpydc catalysts. (b) Proposed mechanism for the formation of formate from the photocatalytic reaction with UiO-67-Mn(bpy)(Co)3Br [110]. (c) CO₂ reduction experiments and methane evolution observed within 6 h of UV-lamp illumination measured after 2, 4 and 6 h for GNP/TiO₂, TiO₂ after pyrolysis of MOF and commercial P25 and Aurolite catalysts [111].

photocatalysts with various phase compositions, size and surface area. Such MOF served as a support matrix for the dispersion of gold nanoparticles (GNPs) and subsequently was utilized as a sacrificial precursor to obtain GNP/TiO₂ nano-composite materials with controllable microstructure. Firstly, GNPs were dispersed and stabilized on NH₂-MIL-125(Ti) with a favored deposition and aggregation of the GNPs on the outer surface of the MOF rather than in the bulk of the MOF. A key step of the fabrication process was the pyrolysis of the resulting GNP/NH₂-MIL-125 at 450 °C to form GNP/TiO₂ and TiO₂; this made it possible to overcome the risk of framework decomposition, which might occur in aqueous environments where most photocatalytic reactions are performed. The photocatalytic reduction of CO₂ to methane under visible light was performed on GNP/TiO₂ and TiO₂ fabricated by pyrolysis of NH₂-MIL-101(Ti), along with a commercial TiO₂ (Fig. 15c). The presence of GNPs in TiO₂ resulted in a higher methane formation with a maximum amount of 62 ppm of CH₄, whereas only 14 ppm of the product was formed with the MOF derived TiO₂ catalyst without deposited GNPs. On the other hand, the utilization of commercial P25 and Aurolite as catalysts resulted in the formation of a lower amount of methane indicating the viability of this preparation method.

5. Conclusions and perspectives

MOFs are a new promising class of crystalline materials with micro/meso-porosity, constituted by the connection of organic linkers and inorganic metal centers. The development of increasingly efficient MOF materials is a key research area in catalysis because of their potential benefits mainly related to the tunable chemical structures and versatile applications. Their application in photocatalytic CO₂ reduction has gained significant attention over the past years due to their intrinsic porosity and smooth implementation of basic moieties which facilitated CO₂ adsorption and efficient light absorption. As highlighted in this review, MOFs can be used in a number of configurations. First, they can be utilized as primary photocatalysts capable of harvesting visible light along with providing active centers for the reduction of CO₂ encompassed in one structure. Their performance can be enhanced through adjusting the organic linkers for more efficient light harvesters, tuning the metal centers to maximize activity, or even a combination of both approaches. Apart from that, the versatility of MOFs allows them to be coupled with semiconductors, while the MOF structure acts as a co-catalyst to promote a higher catalytic activity, or even to be used as an immobilization platform for efficient incorporation of homogeneous catalysts in their structure.

The primary issue faced with the industrial scale application of MOFs in CO₂ reduction is that their current production volume is only limited to substantially small quantities. Generating high-throughput with significant fit for industrial scale is a major hindrance in its future application. Moreover, the performance of MOFs-based photocatalysts is often stymied by low turnover number, as a result of their low electroconductivity and modest accessibility of the reactants to active catalytic sites. When compared to the well-established semiconductor photocatalysts, another observable issue of MOFs is related to their photocatalytic stability. Some works have demonstrated that, although their photocatalytic performance is promising, and in some cases better than that of inorganic semiconductors, their stability is hindered after a number of runs. Overcoming the stability deficiency might spur an interest in further investigations in MOFs application in photocatalytic CO₂ reduction. On the other hand, most of the MOF applications highlighted in this work depended on the use of TEOA as a sacrificial agent among others which is expensive and environmentally unfriendly, this being usually unnecessary in traditional photocatalytic systems. Alternatively, water may be used as electron donor, being non-toxic, environmentally friendly, low cost and easily accessible. However, this is not always possible for different reasons including the hydrogen evolution deriving from water reduction, which may be a competitive reaction hampering the generation of organic fuel from

CO₂. On another level, the development of MOFs for industrial application is economically intensive, at which in their current stage their utilization would hardly be economically sustainable. Given that this field is relatively new, it is expected that the current studies and efforts will stimulate new perspectives in MOF-based photocatalysis for CO₂ reduction and will open for the development of inexpensive, stable, and increasingly efficient MOFs photocatalysts.

Acknowledgments

Funding by Abu Dhabi Education and Knowledge department at the Ministry of Education of United Arab Emirates is gratefully acknowledged (project ADEK Award for Research Excellence 2017, n. 1500000657). This study initiated as a coursework during the PhD-level course “Heterogeneous Catalysis” held at the Khalifa University of Science and Technology.

References

- [1] B. Huskinson, M.P. Marshak, C. Suh, S. Er, M.R. Gerhardt, C.J. Galvin, X. Chen, A. Aspuru-Guzik, R.G. Gordon, M.J. Aziz, A metal-free organic-inorganic aqueous flow battery, *Nature* 505 (2014) 195.
- [2] S.A. Rackley, *Carbon Capture and Storage*, Elsevier, 2009.
- [3] A. Goepfert, M. Czaun, J.-P. Jones, G.K. Surya Prakash, G.A. Olah, Recycling of carbon dioxide to methanol and derived products - closing the loop, *Chem. Soc. Rev.* 43 (2014) 7995–8048.
- [4] T.M. McDonald, J.A. Mason, X. Kong, E.D. Bloch, D. Gygi, A. Dani, V. Crocellà, F. Giordanino, S.O. Odoh, W.S. Drisdell, B. Vlasisavljevic, A.L. Dzubak, R. Poloni, S.K. Schnell, N. Planas, K. Lee, T. Pascal, L.F. Wan, D. Prendergast, J.B. Neaton, B. Smit, J.B. Kortright, L. Gagliardi, S. Bordiga, J.A. Reimer, J.R. Long, Cooperative insertion of CO₂ in diamine-appended metal-organic frameworks, *Nature* 519 (2015) 303.
- [5] J.-R. Li, Y. Ma, M.C. McCarthy, J. Sculley, J. Yu, H.-K. Jeong, P.B. Balbuena, H.-C. Zhou, Carbon dioxide capture-related gas adsorption and separation in metal-organic frameworks, *Coord. Chem. Rev.* 255 (2011) 1791–1823.
- [6] R.V. Demicco, T.K. Lowenstein, L.A. Hardie, Atmospheric pCO₂ since 60 Ma from records of seawater pH, calcium, and primary carbonate mineralogy, *Geology* 31 (2003) 793–796.
- [7] E.S.R.L.a.G.M.D. NOAA Research, Trends in Atmospheric Carbon Dioxide, U.S. Department of Commerce.
- [8] A.S. Agarwal, Y. Zhai, D. Hill, N. Sridhar, The Electrochemical Reduction of Carbon Dioxide to Formate/Formic Acid: Engineering and Economic Feasibility, *ChemSusChem* 4 (2011) 1301–1310.
- [9] K.S. Lackner, Capture of carbon dioxide from ambient air, *Eur. Phys. J. Spec. Top.* 176 (2009) 93–106.
- [10] A. Dhakshinamoorthy, A.M. Asiri, H. Garcia, Catalysis by metal-organic frameworks in water, *Chem. Commun.* 50 (2014) 12800–12814.
- [11] D. Sun, L. Ye, Z. Li, Visible-light-assisted aerobic photocatalytic oxidation of amines to imines over NH₂-MIL-125(Ti), *Appl. Catal. B* 164 (2015) 428–432.
- [12] B. Kumar, M. Lorente, J. Froehlich, T. Dang, A. Sathrum, C.P. Kubiak, Photochemical and photoelectrochemical reduction of CO₂, *Annu. Rev. Phys. Chem.* 63 (2012) 541–569.
- [13] S. Xie, Q. Zhang, G. Liu, Y. Wang, Photocatalytic and photoelectrocatalytic reduction of CO₂ using heterogeneous catalysts with controlled nanostructures, *Chem. Commun.* 52 (2016) 35–59.
- [14] O. Ola, M.M. Maroto-Valer, Review of material design and reactor engineering on TiO₂ photocatalysis for CO₂ reduction, *J. Photochem. Photobiol. C Photochem. Rev.* 24 (2015) 16–42.
- [15] J. Qiao, Y. Liu, F. Hong, J. Zhang, A review of catalysts for the electroreduction of carbon dioxide to produce low-carbon fuels, *Chem. Soc. Rev.* 43 (2014) 631–675.
- [16] S.N. Habisreutinger, L. Schmidt-Mende, J.K. Stolarczyk, Photocatalytic reduction of CO₂ on TiO₂ and other semiconductors, *Angew. Chemie Int. Ed.* 52 (2013) 7372–7408.
- [17] N.S. Lewis, D.G. Nocera, Powering the planet: chemical challenges in solar energy utilization, *Proceedings of the National Academy of Sciences* 103 (2006) 15729–15735.
- [18] K. Li, B. Peng, T. Peng, Recent advances in heterogeneous photocatalytic CO₂ conversion to solar fuels, *ACS Catal.* 6 (2016) 7485–7527.
- [19] S. Wang, X. Wang, Multifunctional Metal–Organic Frameworks for Photocatalysis, *Small* 11 (2015) 3097–3112.
- [20] A. Fujishima, K. Honda, Electrochemical photolysis of water at a semiconductor electrode, *Nature* 238 (1972) 37.
- [21] J. Hou, Z. Wang, W. Kan, S. Jiao, H. Zhu, R.V. Kumar, Efficient visible-light-driven photocatalytic hydrogen production using CdS@TaON core-shell composites coupled with graphene oxide nanosheets, *J. Mater. Chem.* 22 (2012) 7291–7299.
- [22] M. Wang, J. Iocozzia, L. Sun, C. Lin, Z. Lin, Inorganic-modified semiconductor TiO₂ nanotube arrays for photocatalysis, *Energy Environ. Sci.* 7 (2014) 2182–2202.
- [23] L. Xu, J. Xia, K. Wang, L. Wang, H. Li, H. Xu, L. Huang, M. He, Ionic liquid assisted synthesis and photocatalytic properties of [small alpha]-Fe₂O₃ hollow

- microspheres, *J. Chem. Soc. Dalton Trans.* 42 (2013) 6468–6477.
- [24] J. Yu, X. Yu, Hydrothermal synthesis and photocatalytic activity of zinc oxide hollow spheres, *Environ. Sci. Technol.* 42 (2008) 4902–4907.
- [25] Q. Liu, Y.-N. Li, H.-H. Zhang, B. Chen, C.-H. Tung, L.-Z. Wu, Reactivity and mechanistic insight into visible-light-induced aerobic cross-dehydrogenative coupling reaction by organophotocatalysts, *Chem. Eur. J.* 18 (2012) 620–627.
- [26] A. Taheri Najafabadi, Emerging applications of graphene and its derivatives in carbon capture and conversion: current status and future prospects, *Renew. Sustain. Energy Rev.* 41 (2015) 1515–1545.
- [27] J. Yang, D. Wang, H. Han, C. Li, Roles of cocatalysts in photocatalysis and photoelectrocatalysis, *Acc. Chem. Res.* 46 (2013) 1900–1909.
- [28] A.L. Linsebigler, G. Lu, J.T. Yates, Photocatalysis on TiO₂ surfaces: principles, mechanisms, and selected results, *Chem. Rev.* 95 (1995) 735–758.
- [29] M. Wen, K. Mori, Y. Kuwahara, T. An, H. Yamashita, Design and architecture of metal organic frameworks for visible light enhanced hydrogen production, *Appl. Catal. B* 218 (2017) 555–569.
- [30] M. Dilla, R. Schlögl, J. Strunk, Photocatalytic CO₂ reduction under continuous flow high-purity conditions: quantitative evaluation of CH₄ formation in the steady-state, *ChemCatChem* 9 (2017) 696–704.
- [31] X. Li, J. Wen, J. Low, Y. Fang, J. Yu, Design and fabrication of semiconductor photocatalyst for photocatalytic reduction of CO₂ to solar fuel, *Sci. China Mater.* 57 (2014) 70–100.
- [32] M.A. Nasalevich, M. van der Veen, F. Kapteijn, J. Gascon, Metal-organic frameworks as heterogeneous photocatalysts: advantages and challenges, *CrystEngComm* 16 (2014) 4919–4926.
- [33] W. Tu, Y. Zhou, Z. Zou, Photocatalytic conversion of CO₂ into renewable hydrocarbon fuels: state-of-the-art accomplishment, challenges, and prospects, *Adv. Mater.* 26 (2014) 4607–4626.
- [34] A. Hagfeldt, G. Boschloo, L. Sun, L. Kloo, H. Pettersson, Dye-sensitized solar cells, *Chem. Rev.* 110 (2010) 6595–6663.
- [35] W.J. Youngblood, S.-H.A. Lee, Y. Kobayashi, E.A. Hernandez-Pagan, P.G. Hoertz, T.A. Moore, A.L. Moore, D. Gust, T.E. Mallouk, Photoassisted overall water splitting in a visible light-absorbing dye-sensitized photoelectrochemical cell, *J. Am. Chem. Soc.* 131 (2009) 926–927.
- [36] H. He, J.A. Perman, G. Zhu, S. Ma, Metal-organic frameworks for CO₂ chemical transformations, *Small* 12 (2016) 6309–6324.
- [37] M.H. Beyzavi, C.J. Stephenson, Y. Liu, O. Karagiari, J.T. Hupp, O.K. Farha, Metal-organic framework-based catalysts: chemical fixation of CO₂ with epoxides leading to cyclic organic carbonates, *Front. Energy Res.* 2 (2015).
- [38] H.-Y. Wang, F.-X. Xiao, L. Yu, B. Liu, X.W. Lou, Hierarchical α-MnO₂ nanowires@Ni_{1-x}Mn_xO₂ nanoflakes core-shell nanostructures for supercapacitors, *Small* 10 (2014) 3181–3186.
- [39] J.-L. Wang, C. Wang, W. Lin, Metal-organic frameworks for light harvesting and photocatalysis, *ACS Catal.* 2 (2012) 2630–2640.
- [40] S. Hasegawa, S. Horike, R. Matsuda, S. Furukawa, K. Mochizuki, Y. Kinoshita, S. Kitagawa, Three-dimensional porous coordination polymer functionalized with amide groups based on tridentate ligand: selective sorption and catalysis, *J. Am. Chem. Soc.* 129 (2007) 2607–2614.
- [41] D. Jiang, T. Mallat, F. Krumeich, A. Baiker, Copper-based metal-organic framework for the facile ring-opening of epoxides, *J. Catal.* 257 (2008) 390–395.
- [42] K.V. Kovtunov, V.V. Zhivonitko, A. Corma, I.V. Koptuyg, Parahydrogen-induced polarization in heterogeneous hydrogenations catalyzed by an immobilized au(III) complex, *J. Phys. Chem. Lett.* 1 (2010) 1705–1708.
- [43] C.-C. Wang, Y.-Q. Zhang, J. Li, P. Wang, Photocatalytic CO₂ reduction in metal-organic frameworks: a mini review, *J. Mol. Struct.* 1083 (2015) 127–136.
- [44] S. Zhang, L. Li, S. Zhao, Z. Sun, M. Hong, J. Luo, Hierarchical metal-organic framework nanoflowers for effective CO₂ transformation driven by visible light, *J. Mater. Chem. A* 3 (2015) 15764–15768.
- [45] S. Kitagawa, R. Kitaura, S.-i. Noro, Functional porous coordination polymers, *Angew. Chemie Int. Ed.* 43 (2004) 2334–2375.
- [46] M. Alvaro, E. Carbonell, B. Ferrer, F.X. Llabrés i Xamena, H. Garcia, Semiconductor behavior of a metal-organic framework (MOF), *Chem. Eur. J.* 13 (2007) 5106–5112.
- [47] T. Zhang, W. Lin, Metal-organic frameworks for artificial photosynthesis and photocatalysis, *Chem. Soc. Rev.* 43 (2014) 5982–5993.
- [48] C. Gomes Silva, I. Luz, F.X. Llabrés i Xamena, A. Corma, H. García, Water stable Zr-benzenedicarboxylate metal-organic frameworks as photocatalysts for hydrogen generation, *Chem. Eur. J.* 16 (2010) 11133–11138.
- [49] Y. Horiuchi, T. Toyao, M. Saito, K. Mochizuki, M. Iwata, H. Higashimura, M. Anpo, M. Matsuoka, Visible-light-promoted photocatalytic hydrogen production by using an amino-functionalized Ti(IV) metal-organic framework, *J. Phys. Chem. C* 116 (2012) 20848–20853.
- [50] S. Bordiga, C. Lamberti, G. Ricchiardi, L. Regli, F. Bonino, A. Damin, K.P. Lillerud, M. Bjorgen, A. Zecchina, Electronic and vibrational properties of a MOF-5 metal-organic framework: ZnO quantum dot behaviour, *Chem. Commun.* (2004) 2300–2301.
- [51] C.A. Kent, D. Liu, L. Ma, J.M. Papanikolas, T.J. Meyer, W. Lin, Light harvesting in microscale metal-organic frameworks by energy migration and interfacial electron transfer quenching, *J. Am. Chem. Soc.* 133 (2011) 12940–12943.
- [52] C.A. Kent, D. Liu, T.J. Meyer, W. Lin, Amplified luminescence quenching of phosphorescent metal-organic frameworks, *J. Am. Chem. Soc.* 134 (2012) 3991–3994.
- [53] C.A. Kent, B.P. Mehl, L. Ma, J.M. Papanikolas, T.J. Meyer, W. Lin, Energy transfer dynamics in metal-organic frameworks, *J. Am. Chem. Soc.* 132 (2010) 12767–12769.
- [54] G. Wang, Q. Sun, Y. Liu, B. Huang, Y. Dai, X. Zhang, X. Qin, A bismuth-based metal-organic framework as an efficient visible-light-driven photocatalyst, *Chem. Eur. J.* 21 (2015) 2364–2367.
- [55] B.M. Rajbongshi, S.K. Samdarshi, Cobalt-doped zincblende-wurtzite mixed-phase ZnO photocatalyst nanoparticles with high activity in visible spectrum, *Appl. Catal. B* 144 (2014) 435–441.
- [56] S. Subudhi, D. Rath, K.M. Parida, A mechanistic approach towards the photocatalytic organic transformations over functionalised metal organic frameworks: a review, *Catal. Sci. Technol.* (2018).
- [57] X. Kong, H. Deng, F. Yan, J. Kim, J.A. Swisher, B. Smit, O.M. Yaghi, J.A. Reimer, Mapping of functional groups in metal-organic frameworks, *Science* 341 (2013) 882.
- [58] Y. Fu, D. Sun, Y. Chen, R. Huang, Z. Ding, X. Fu, Z. Li, An amine-functionalized titanium metal-organic framework photocatalyst with visible-light-induced activity for CO₂ reduction, *Angew. Chemie* 124 (2012) 3420–3423.
- [59] B. Arstad, H. Fjellvåg, K.O. Kongshaug, O. Swang, R. Blom, Amine functionalised metal organic frameworks (MOFs) as adsorbents for carbon dioxide, *Adsorption* 14 (2008) 755–762.
- [60] D. Sun, Y. Fu, W. Liu, L. Ye, D. Wang, L. Yang, X. Fu, Z. Li, Studies on photocatalytic CO₂ reduction over NH₂-Uio-66(Zr) and its derivatives: towards a better understanding of photocatalysis on metal-organic frameworks, *Chem. Eur. J.* 19 (2013) 14279–14285.
- [61] D. Wang, R. Huang, W. Liu, D. Sun, Z. Li, Fe-based MOFs for photocatalytic CO₂ reduction: role of coordination unsaturated sites and dual excitation pathways, *ACS Catal.* 4 (2014) 4254–4260.
- [62] S. More, R. Bhosale, A. Mateo-Alonso, Low-LUMO pyrene-fused azacenes, *Chem. Eur. J.* 20 (2014) 10626–10631.
- [63] M. Sun, S. Yan, Y. Sun, X. Yang, Z. Guo, J. Du, D. Chen, P. Chen, H. Xing, Enhancement of visible-light-driven CO₂ reduction performance using an amine-functionalized zirconium metal-organic framework, *J. Chem. Soc. Dalton Trans.* (2018).
- [64] D. Chen, H. Xing, C. Wang, Z. Su, Highly efficient visible-light-driven CO₂ reduction to formate by a new anthracene-based zirconium MOF via dual catalytic routes, *J. Mater. Chem. A* 4 (2016) 2657–2662.
- [65] W.-Y. Gao, M. Chrzanowski, S. Ma, Metal-metalloporphyrin frameworks: a resurging class of functional materials, *Chem. Soc. Rev.* 43 (2014) 5841–5866.
- [66] H.-Q. Xu, J. Hu, D. Wang, Z. Li, Q. Zhang, Y. Luo, S.-H. Yu, H.-L. Jiang, visible-light photoreduction of CO₂ in a metal-organic framework: boosting electron-hole separation via electron trap states, *J. Am. Chem. Soc.* 137 (2015) 13440–13443.
- [67] N. Sadeghi, S. Sharifnia, M. Sheikh Arabi, A porphyrin-based metal organic framework for high rate photoreduction of CO₂ to CH₄ in gas phase, *J. Co2 Util.* 16 (2016) 450–457.
- [68] Y. Ji, Y. Luo, Theoretical study on the mechanism of photoreduction of CO₂ to CH₄ on the anatase TiO₂(101) surface, *ACS Catal.* 6 (2016) 2018–2025.
- [69] P. Akhter, H. Hussain, G. Saracco, N. Russo, Novel nanostructured-TiO₂ materials for the photocatalytic reduction of CO₂ greenhouse gas to hydrocarbons and syngas, *Fuel* 149 (2015) 55–65.
- [70] S.J.A. Pope, B.J. Coe, S. Faulkner, E.V. Bichenkova, X. Yu, K.T. Douglas, Self-assembly of heterobimetallic d-f hybrid complexes: sensitization of lanthanide luminescence by d-block metal-to-ligand charge-transfer excited states, *J. Am. Chem. Soc.* 126 (2004) 9490–9491.
- [71] L. Li, S. Zhang, L. Xu, J. Wang, L.-X. Shi, Z.-N. Chen, M. Hong, J. Luo, Effective visible-light driven CO₂ photoreduction via a promising bifunctional iridium coordination polymer, *Chem. Sci.* 5 (2014) 3808–3813.
- [72] L.B. Vilhelmsen, K.S. Walton, D.S. Sholl, Structure and mobility of metal clusters in MOFs: Au, Pd, and AuPd clusters in MOF-74, *J. Am. Chem. Soc.* 134 (2012) 12807–12816.
- [73] P. Horcajada, S. Surlle, C. Serre, D.-Y. Hong, Y.-K. Seo, J.-S. Chang, J.-M. Greneche, I. Margiolaki, G. Férey, Synthesis and catalytic properties of MIL-100(Fe), an iron(III) carboxylate with large pores, *Chem. Commun.* (2007) 2820–2822.
- [74] G. Férey, C. Mellot-Draznieks, C. Serre, F. Millange, J. Dutour, S. Surlblé, I. Margiolaki, A chromium terephthalate-based solid with unusually large pore volumes and surface area, *Science* 309 (2005) 2040.
- [75] C. Mellot-Draznieks, C. Serre, S. Surlblé, N. Audebrand, G. Férey, Very large swelling in hybrid frameworks: a combined computational and powder diffraction study, *J. Am. Chem. Soc.* 127 (2005) 16273–16278.
- [76] P. Horcajada, F. Salles, S. Wuttke, T. Devic, D. Heurtaux, G. Maurin, A. Vimont, M. Daturi, O. David, E. Magnier, N. Stock, Y. Filinchuk, D. Popov, C. Riekel, G. Férey, C. Serre, How Linker's modification controls swelling properties of highly flexible iron(III) dicarboxylates MIL-88, *J. Am. Chem. Soc.* 133 (2011) 17839–17847.
- [77] M.R. Lohe, M. Rose, S. Kaskel, Metal-organic framework (MOF) aerogels with high micro- and macroporosity, *Chem. Commun.* (2009) 6056–6058.
- [78] K.G.M. Laurier, F. Vermoortele, R. Ameloot, D.E. De Vos, J. Hofkens, M.B.J. Roeffaers, Iron(III)-based metal-organic frameworks as visible light photocatalysts, *J. Am. Chem. Soc.* 135 (2013) 14488–14491.
- [79] S. Bordiga, R. Buzzoni, F. Geobaldo, C. Lamberti, E. Giamello, A. Zecchina, G. Leofanti, G. Petrini, G. Tozzola, G. Vlaic, Structure and reactivity of framework and extraframework iron in Fe-Silicalite as investigated by spectroscopic and physicochemical methods, *J. Catal.* 158 (1996) 486–501.
- [80] Y. Li, Z. Feng, H. Xin, F. Fan, J. Zhang, P.C.M.M. Magusin, E.J.M. Hensen, R.A. van Santen, Q. Yang, C. Li, Effect of aluminum on the nature of the Iron species in Fe-SBA-15, *J. Phys. Chem. B* 110 (2006) 26114–26121.
- [81] Y. Li, W.-N. Wang, Z. Zhan, M.-H. Woo, C.-Y. Wu, P. Biswas, Photocatalytic reduction of CO₂ with H₂O on mesoporous silica supported Cu/TiO₂ catalysts, *Appl. Catal. B* 100 (2010) 386–392.

- [82] H. Zhang, J. Wei, J. Dong, G. Liu, L. Shi, P. An, G. Zhao, J. Kong, X. Wang, X. Meng, J. Zhang, J. Ye, Efficient visible-light-driven carbon dioxide reduction by a single-atom implanted metal–organic framework, *Angew. Chemie Int. Ed.* 55 (2016) 14310–14314.
- [83] W. Lin, H. Frei, Photochemical CO₂ Splitting by metal-to-metal charge-transfer excitation in mesoporous ZrCu(I)-MCM-41 silicate sieve, *J. Am. Chem. Soc.* 127 (2005) 1610–1611.
- [84] I.H. Tseng, W.-C. Chang, J.C.S. Wu, Photoreduction of CO₂ using sol–gel derived titania and titania-supported copper catalysts, *Appl. Catal. B* 37 (2002) 37–48.
- [85] I.H. Tseng, J.C.S. Wu, H.-Y. Chou, Effects of sol–gel procedures on the photocatalysis of Cu/TiO₂ in CO₂ photoreduction, *J. Catal.* 221 (2004) 432–440.
- [86] Y. Liu, Y. Yang, Q. Sun, Z. Wang, B. Huang, Y. Dai, X. Qin, X. Zhang, Chemical adsorption enhanced CO₂ capture and photoreduction over a copper porphyrin based metal organic framework, *ACS Appl. Mater. Interfaces* 5 (2013) 7654–7658.
- [87] Y. Huang, Z. Zheng, Z. Ai, L. Zhang, X. Fan, Z. Zou, Core–shell microspherical Ti_{1-x}Zr_xO₂ solid solution photocatalysts directly from ultrasonic spray pyrolysis, *J. Phys. Chem. B* 110 (2006) 19323–19328.
- [88] I. Tsuji, H. Kato, H. Kobayashi, A. Kudo, Photocatalytic H₂ evolution reaction from aqueous solutions over band structure-controlled (AgIn)_xZn_{2(1-x)}S₂ solid solution photocatalysts with visible-light response and their surface nanostructures, *J. Am. Chem. Soc.* 126 (2004) 13406–13413.
- [89] W. Zhang, Z. Zhong, Y. Wang, R. Xu, Doped solid solution: (Zn_{0.95}Cu_{0.05})_{1-x}Cd_xS nanocrystals with high activity for H₂ evolution from aqueous solutions under visible light, *J. Phys. Chem. C* 112 (2008) 17635–17642.
- [90] H. Han, H. Frei, Controlled assembly of hetero-binuclear sites on mesoporous silica: visible light charge-transfer units with selectable redox properties, *J. Phys. Chem. C* 112 (2008) 8391–8399.
- [91] R. Nakamura, A. Okamoto, H. Osawa, H. Irie, K. Hashimoto, Design of all-inorganic molecular-based photocatalysts sensitive to visible light: Ti(IV)–O–Ce(III) bimetallic assemblies on mesoporous silica, *J. Am. Chem. Soc.* 129 (2007) 9596–9597.
- [92] C.K. Brozek, M. Dincă, Ti³⁺, V^{2+/3+}, Cr^{2+/3+}, Mn²⁺, and Fe²⁺-Substituted MOF-5 and redox reactivity in Cr- and Fe-MOF-5, *J. Am. Chem. Soc.* 135 (2013) 12886–12891.
- [93] M. Kim, J.F. Cahill, H. Fei, K.A. Prather, S.M. Cohen, Postsynthetic ligand and cation exchange in robust metal–organic frameworks, *J. Am. Chem. Soc.* 134 (2012) 18082–18088.
- [94] W. Liang, R. Babarao, D.M. D'Alessandro, Microwave-assisted solvothermal synthesis and optical properties of tagged MIL-140A metal–organic frameworks, *Inorg. Chem.* 52 (2013) 12878–12880.
- [95] L. Valenzano, B. Civalleri, S. Chavan, S. Bordiga, M.H. Nilsen, S. Jakobsen, K.P. Lillerud, C. Lamberti, Disclosing the complex structure of UiO-66 metal organic framework: a synergic combination of experiment and theory, *Chem. Mater.* 23 (2011) 1700–1718.
- [96] F. Vermoortele, B. Bueken, G. Le Bars, B. Van de Voorde, M. Vandichel, K. Houthoofd, A. Vimont, M. Daturi, M. Waroquier, V. Van Speybroeck, C. Kirschhock, D.E. De Vos, Synthesis modulation as a tool to increase the catalytic activity of metal–organic frameworks: The unique case of UiO-66(Zr), *J. Am. Chem. Soc.* 135 (2013) 11465–11468.
- [97] Q. Yang, A.D. Wiersum, P.L. Llewellyn, V. Guillerm, C. Serre, G. Maurin, Functionalizing porous zirconium terephthalate UiO-66(Zr) for natural gas upgrading: a computational exploration, *Chem. Commun.* 47 (2011) 9603–9605.
- [98] D. Sun, W. Liu, M. Qiu, Y. Zhang, Z. Li, Introduction of a mediator for enhancing photocatalytic performance via post-synthetic metal exchange in metal-organic frameworks (MOFs), *Chem. Commun.* 51 (2015) 2056–2059.
- [99] Y. Lee, S. Kim, J.K. Kang, S.M. Cohen, Photocatalytic CO₂ reduction by a mixed metal (Zr/Ti), mixed ligand metal-organic framework under visible light irradiation, *Chem. Commun.* 51 (2015) 5735–5738.
- [100] Y. Lee, S. Kim, H. Fei, J.K. Kang, S.M. Cohen, Photocatalytic CO₂ reduction using visible light by metal-monocatecholato species in a metal-organic framework, *Chem. Commun.* 51 (2015) 16549–16552.
- [101] Y.-F. Li, D. Xu, J.I. Oh, W. Shen, X. Li, Y. Yu, Mechanistic study of Codoped titania with nonmetal and metal ions: a case of C + Mo codoped TiO₂, *ACS Catal.* 2 (2012) 391–398.
- [102] L. Rui, H. Jiahua, D. Mingsen, W. Helin, W. Xijun, H. Yingli, J. Hai-Long, J. Jun, Z. Qun, X. Yi, X. Yujie, Integration of an inorganic semiconductor with a metal–organic framework: a platform for enhanced gaseous photocatalytic reactions, *Adv. Mater.* 26 (2014) 4783–4788.
- [103] Q. Liu, Z.-X. Low, L. Li, A. Razmjou, K. Wang, J. Yao, H. Wang, ZIF-8/Zn₂GeO₄ nanorods with an enhanced CO₂ adsorption property in an aqueous medium for photocatalytic synthesis of liquid fuel, *J. Mater. Chem. A* 1 (2013) 11563–11569.
- [104] Y. Su, Z. Zhang, H. Liu, Y. Wang, Cd_{0.2}Zn_{0.8}S@UiO-66-NH₂ nanocomposites as efficient and stable visible-light-driven photocatalyst for H₂ evolution and CO₂ reduction, *Appl. Catal. B* 200 (2017) 448–457.
- [105] W. Sibó, Y. Wangshu, L. Jinliang, D. Zhengxin, W. Xinchun, Cobalt imidazolate metal–organic frameworks photosplit CO₂ under mild reaction conditions, *Angew. Chemie Int. Ed.* 53 (2014) 1034–1038.
- [106] S. Wang, J. Lin, X. Wang, Semiconductor-redox catalysis promoted by metal-organic frameworks for CO₂ reduction, *J. Chem. Soc. Faraday Trans.* 16 (2014) 14656–14660.
- [107] S. Wang, X. Wang, Photocatalytic CO₂ reduction by CdS promoted with a zeolitic imidazolate framework, *Appl. Catal. B* 162 (2015) 494–500.
- [108] F. Dawei, W. Kecheng, S. Jie, L. Tian-Fu, P. Jihye, W. Zhangwen, B. Mathieu, Y. Andrey, Z. Xiaodong, Z. Hong-Cai, A highly stable zeotype mesoporous zirconium metal–organic framework with ultralarge pores, *Angew. Chemie Int. Ed.* 54 (2015) 149–154.
- [109] C.M. B., W. Xia, E. Noémie, H.C. H., W. Aron, B. Jonathan, C. Jérôme, Q.E. Alessandra, F. David, M.D. Caroline, F. Marc, Photocatalytic Carbon Dioxide Reduction with Rhodium-based Catalysts in Solution and Heterogenized within Metal–Organic Frameworks, *ChemSusChem*, 8 (2015) 603–608.
- [110] H. Fei, M.D. Sampson, Y. Lee, C.P. Kubiak, S.M. Cohen, photocatalytic CO₂ reduction to formate using a Mn(I) molecular catalyst in a robust metal–organic framework, *Inorg. Chem.* 54 (2015) 6821–6828.
- [111] K. Khaletskaya, A. Pougin, R. Medishetty, C. Rösler, C. Wiktor, J. Strunk, R.A. Fischer, fabrication of gold/titania photocatalyst for CO₂ reduction based on pyrolytic conversion of the metal–organic framework NH₂-MIL-125(Ti) loaded with gold nanoparticles, *Chem. Mater.* 27 (2015) 7248–7257.